(Presented at the 3rd International
Conf. on High Energy Collisions,
Stony Brook, N.Y., Sept. 5-6, 1969.)

SLAC-PUB-660
September 1969
(TH) and (EXP)

INELASTIC ELECTRON-PROTON SCATTERING*

L. W. Mo†

Stanford Linear Accelerator Center
Stanford University, Stanford, California 94305

Electron-proton inelastic scattering experiments can provide valuable information on the electromagnetic interactions of the hadrons. The specific subjects one can learn from these experiments are the following:

1. The variation of the form factors at the γNW vertex as a function of the four-momentum transfer squared, q^2. Here W designates the invariant mass of the final hadronic system.
2. The axial vector form factor, $G_A(q^2)$, by studying the electroproduction near the pion threshold.[1]
3. The total photon-proton absorption cross section by extrapolation to the limit of $q^2 \to 0$.
4. Test of various sum rules on the process: γ(off-mass-shell) + proton $\longrightarrow$ hadrons.[2]
5. Test of time reversal invariance in electromagnetic interactions of hadrons if the proton target is polarized.[3]

In this report, the majority of the results is based on the experiments done at SLAC as carried out by a SLAC-MIT collaboration.[4-7] In order to define the notations used, the kinematics and conventional expressions for the cross sections will first be introduced. Then a discussion of the experiments and implications of the data will follow.

---

*Work supported by the U.S. Atomic Energy Commission.

†Permanent address (after September 1969): The Enrico Fermi Institute and the Department of Physics, The University of Chicago, Chicago, Illinois.

I. Kinematics and Cross Section Formula

In the approximation of a one-photon exchange between the electron and the proton current, the differential cross section for detecting only the scattered electrons can be expressed as[8]:

$$\frac{d^2\sigma}{d\Omega dE'} = \left(\frac{d\sigma}{d\Omega}\right)_{Mott} \left[W_2(q^2, W) + 2W_1(q^2), W) \tan^2 \theta/2\right]$$

where

$$\left(\frac{d\sigma}{d\Omega}\right)_{Mott} = \frac{\alpha^2 \cos^2 \theta/2}{4E_0^2 \sin^4 \theta/2} \quad ,$$

θ = scattering angle of the electron in laboratory system,

E_0 = incident electron energy in laboratory system,

$E' = \dfrac{E_0 - K}{1 + \dfrac{2E_0}{M_p} \sin^2 \theta/2}$ = scattered electron energy in laboratory system,

$q^2 = 4E_0E' \sin^2 \theta/2$ = four-momentum-transfer squared of the virtual photon,

$\nu = E_0 - E' = q_0$ = the energy transfer to the target,

$K = \dfrac{\left(W^2 - M_p^2\right)}{2M_p} = \nu - \dfrac{q^2}{2M_p}$ = equivalent real photon energy needed to photoproduce a final hadronic system of mass W from a proton target,

M_p = rest mass of proton,

W = invariant mass of the final hadronic system,

W_1, W_2 = two form factors to be determined by experiments,[9]

and $\alpha = \dfrac{1}{137}$ = the fine structure constant.

Another useful representation, originally due to Hand,[10] is to express the e-p scattering cross section in terms of the interaction cross sections of the transversely and the longitudinally polarized virtual photon as follows:

$$\frac{d^2\sigma}{d\Omega dE'} = \Gamma_t(E_0, E', \theta) \left[\sigma_T(q^2, W) + \epsilon\, \sigma_L(q^2, W)\right]$$

where

$$\Gamma_t(E_0, E', \theta) = \frac{\alpha}{2\pi^2} \left(\frac{K}{q^2}\right) \left(\frac{E'}{E_0}\right) \frac{1}{1-\epsilon} \quad ,$$

= the virtual photon spectrum,

$$\epsilon = \frac{1}{1 + 2\left(1 + \frac{\nu^2}{q^2}\right) \tan^2 \theta/2} \quad ,$$

$\sigma_T(q^2, W)$ = total photon-proton interaction cross section of the transversely polarized virtual photon (i.e., the polarization direction is perpendicular to that of $\vec{q}$),

and

$\sigma_L(q^2, W)$ = total photon-proton interaction cross section of the longitudinally polarized virtual photon (i.e., the polarization direction is along that of $\vec{q}$).

In the limit of $q^2 \to 0$, the transverse cross section approaches the total photoabsorption cross section $\sigma_{\gamma p}(W)$. This offers another possibility for obtaining information on $\sigma_{\gamma p}$ at high energies by extrapolating the data of electroproduction experiments as they have the advantage of faster data acquisition.

The relationship between the two above-mentioned representations is given[11] as below:

$$W_1(q^2, W) = \frac{K}{4\pi^2 \alpha}\, \sigma_T(q^2, W) \quad ,$$

$$W_2(q^2, W) = \frac{K}{4\pi^2\alpha}\left(\frac{q^2}{q^2 + \nu^2}\right)\left[\sigma_T(q^2, W) + \sigma_L(q^2, W)\right] ,$$

and

$$\frac{W_1(q^2, W)}{W_2(q^2, W)} = \left(1 + \frac{\nu^2}{q^2}\right) \frac{\sigma_T(q^2, W)}{\left[\sigma_T(q^2, W) + \sigma_L(q^2, W)\right]} .$$

II. The SLAC-MIT Experiment[4-7]

In the SLAC-MIT experiment, high energy electrons from the two-mile long linear accelerator were momentum analyzed and sent through a 7 cm long liquid hydrogen target. The scattered electrons were momentum analyzed and detected by either the 20-GeV/c or the 8-GeV/c magnetic spectrometer facilities of SLAC.[12] The momentum and angular resolution of these spectrometers were 0.1% and 0.3 milli-radians respectively. The detectors of each spectrometer consisted mainly of two scintillation hodoscopes located at two different focal planes of the spectrometer to measure the momentum and the scattering angle, a lucite-lead sandwich shower counter of 16 radiation lengths, and three dE/dx counters. For the experiments using the 8-GeV/c spectrometer, an additional threshold-type gas Cerenkov counter was used to help the pion rejection when the scattered electron energy was less than 3 GeV. The master trigger to the electronic system was provided either by a coincidence between two trigger counters or by a signal from the shower counter. Since the beam spill was only 1.6 micro-seconds long, the electronic system was gated off immediately after the occurrence of a master trigger to allow a data rate of at most one event per beam pulse. The contents of the hodoscopes and the pulse height measuring devices were then recorded onto magnetic tapes for later off-line analysis on an event-by-event basis. During the course of the experiment, part of the data were analyzed by an on-line SDS-9300 computer, and the preliminary results were displayed on a scope for immediate

monitoring purposes. The integrated charge of the incident electron beam was measured by two induction toroids and two secondary emission monitors. During part of the experiment, the 1.6-GeV/c spectrometer at SLAC was also used to monitor the recoiling protons from elastic scattering as an auxiliary check. The accuracy on the integrated charge was estimated to be better than 0.5%.

The manner of data-taking was dictated by the requirement of radiative corrections,[13] which is a very important factor for all electron scattering experiments. Since the measurement at each value of incident electron energy, E_0, and scattered electron energy, E', contains the radiative contributions from the entire kinematically accessible region of higher E' and lower E_0, the removal of these radiation contributions requires the complete knowledge of the non-radiative cross sections in the whole kinematically possible region of (E_0, E'). For example, as shown in Fig. 1, it is necessary to know the non-radiative cross sections in the shaded triangle abc in order to radiatively correct the measured cross section at point c. Therefore, at a fixed scattering angle θ, several spectra had to be measured at a few incident electron energies in order to allow a proper interpolation or extrapolation for the sake of radiative corrections.

At SLAC, measurements have been done at scattering angles of 1.5°, 6°, and 10°, using the 20-GeV/c spectrometer; and at 18°, 26°, and 34°, using the 8-GeV/c spectrometer with incident electron energies in the range from 4.5 to 20 GeV. The cross sections were measured at values of E' ranging from 3 GeV up to the elastic peak when using the 20-GeV/c spectrometer; and 1 GeV up to the elastic peak when using the 8-GeV/c spectrometer. Normally, full and dummy target measurements were taken at each setting of the magnetic spectrometer. At the low energy end of each spectrum, the contaminations due to Dalitz pairs were measured by reversing the magnet polarities of the spectrometer. In general, these backgrounds were not important.

In Figs. 2 and 3, four typical experimental spectra already radiatively corrected are shown. The details concerning the radiative corrections can be found in Ref. 13, and will not be repeated here. From these results, the following apparent features can be observed:

1. At low values of q^2, the three nucleon resonances at mass values of 1.238-, 1.512-, and 1.688-GeV were prominently excited. The N* at 1.920-GeV was only weakly excited.
2. As values of q^2 increase, the cross sections in the resonance region decrease very rapidly.
3. As values of q^2 increase, the cross section in the deep inelastic region start to rise as a function of W. It increases at approximately a linear rate when the q^2 value is moderate. But, at high q^2 values, the cross section starts to rise exponentially.

III. Cross Section in the Region of the Nucleon Resonances

Since only the scattered electrons were detected in the SLAC-MIT experiment, the decomposition of the observed cross sections into resonance and non-resonant background was by no means straightforward. A numerical approach was adopted to resolve this problem. The method was to fit an experimental spectrum numerically with a number of Breit-Wigner functions for the resonances actually observed, and a polynomial function to represent the non-resonant background. Since there were no prior reasons for restricting the order of the polynomial function, the fitting procedure allowed a varying order for it. Then the total cross section for each individual resonance, obtained from a non-linear least-square fitting program, was plotted against the number of parameters used for the background. If the order of the polynomial function was too low or too high, the cross sections obtained by the fitting program showed a rapid variation in magnitudes. But when the number

of parameters used for the background was between four and fifteen, the cross sections for the resonances became fairly constant. This stabilized constant region was taken as an answer to the resonance cross section, and the scatter of points provided the uncertainty introduced by the numerical fitting procedure. The detail is given as the following.

A. Numerical Fitting Procedure

The differential cross section, $d^2\sigma/d\Omega dE'$, was numerically fitted by the following expression:

$$\frac{d^2\sigma}{d\Omega dE'} = \sum_{i=0}^{N} C_i W^i$$

$$+ H_1 \left[\frac{W M_{33} \Gamma_1}{\left(W^2 - M_{33}^2\right)^2 + \left(\Gamma_1 M_{33}\right)^2} \right]$$

$$+ \sum_{i=2}^{4} H_i \left[\frac{1}{\left(W - M_i\right)^2 + \left(\Gamma_i/2\right)^2} \right] ,$$

where the polynomial function represents the non-resonant background, and M_i, Γ_i = mass, and width of the i-th resonance,

$$\Gamma_1 = \Gamma_{33} \frac{(0.85\ P_\pi/m_\pi)^3}{\left[1 + (0.85\ P_\pi/m_\pi)^2\right]}$$

P_π = pion momentum in the rest frame of the resonance,

m_π = rest mass of pion, and

H_i = height of the i-th resonance cross section.

The variables, C_i, H_i, M_i, and Γ_i, were treated as adjustable parameters by a non-linear fitting computer program.

It is to be noted that the (33) resonance was treated differently from all the others. An invariant Breit-Wigner function, containing the correct threshold behavior and the proper asymmetric shape, was used for its description because it is predominantly a P_{33} wave. For each of the higher resonances, there are at least four partial waves closely packed together. To simplify such complications, a symmetric and non-relativistic form of the Breit-Wigner function was used for their description.

In Fig. 4, a typical radiatively corrected spectrum is shown together with the resonances and background determined by the fitting procedure. The chi-square value per degree of freedom for these fits had a typical value of approximately 1.05. The non-resonant background obtained this way always had a shape resembling a many-particle phase space.

B. Results and Comparison with Theory

Cross sections for the resonance are listed in Table 1. Values of their masses, widths and the associated errors were obtained from the numerical fits. Errors assigned to the cross sections are the combined values of the statistical error and that introduced by the numerical fitting procedure. It is to be noted that the width determined for the second nucleon isobar thus obtained is only (77 ± 15) MeV, considerably smaller than that given by the pion-nucleon experiment.

In Fig. 5 through Fig. 7, we have plotted the ratio $(d\sigma/d\Omega)/(d\sigma/d\Omega)_{elastic}$ against q^2 for the first three nucleon resonances. The elastic electron-proton scattering cross section, $(d\sigma/d\Omega)_{elastic}$, was computed with the dipole form factors at the same incident electron energy and scattering angle as that used in the measurement. The value used for q^2 was the momentum transfer squared at the

resonance peak. In these plots, the energy and angular dependence were almost completely removed, and the ratio became approximately a function of q^2 only. The solid curves shown are the theoretical predictions of a model given by Walecka and co-workers.[14,15] In that model, only Feynman graphs for (1) direct pion production, (2) one-pion exchange, (3) one-nucleon exchange, (4) one-ω exchange, and, (5) the excitation of a $|\pi N^*_{33}>$ channel for the higher resonances, were included. Four normalization constants involved in the calculation could be fixed by the photoproduction data. Only one adjustable parameter, named β, is left in that theory which is proportional to the ωN coupling strength. The data appeared to be in good agreement with the predictions using $\beta = -6$ and without the $|\pi N^*_{33}>$ channel for the higher resonances. This indicates that the q^2-dependence for the resonance cross section in the region beyond threshold is approximately scaled to that for elastic scattering. However, the effective form factor of the resonance, as evidenced by the data on the (33) resonance, is falling off with increasing q^2 more rapidly than the nucleon form factor.[17-20]

Presently, there is not enough data available to compare with the detailed predictions of Walecka et al. on the Coulomb and transverse form factors.[14,15] The results[20-22] for the longitudinal cross section of the (33) resonance are shown in Fig. 8. For the 1.512-GeV resonance, the longitudinal cross sections in the range of q^2 from 0.1 to 0.6 $(GeV/c)^2$ are nearly zero as measured by Lynch et al.[20] The results on W_1 and W_2 in the resonance region, measured by Albrecht et al.,[23] are shown in Figs. 9 and 10.

IV. Cross Section in the Deep Inelastic Region

As illustrated in Fig. 3, at high q^2, the e-p inelastic scattering cross section, measured at fixed incident electron energy and scattering angle, was observed to be rising with increasing values of W. This observation is consistent with the

inequality relationship given by Bjorken,[2]

$$\lim_{q^2 \to \infty} \left(\frac{d\sigma^{\text{proton}}}{dq^2} + \frac{d\sigma^{\text{neutron}}}{dq^2} \right) \geq \frac{1}{2} \left(\frac{d\sigma}{dq^2} \right)^{\text{point charge}} ,$$

which implies that at infinite momentum transfer the form factors in the deep inelastic region should approach that of a point charge. This tendency is also indicated by the curves shown in Fig. 11, where the 10° data was divided by the Mott cross section and the ratios plotted against q^2. Similar quantities for elastic scattering, calculated with $\theta = 10^{\circ}$ and dipole form factors, are also included in that figure. It can be seen that the inelastic form factors have a much weaker q^2 dependence than those of elastic scattering, and this q^2 dependence decreases as W increases. Presently, there exist only very little information on the individual form factors, W_1 and W_2.[23] Questions on whether these form factors should fall off like $1/q^4$ or $1/q^2$ have to be investigated.

Bjorken originally suggested that, at large values of ν and q^2, the function νW_2 could manifest a property of scale invariance.[24-27] That is, νW_2 could be a universal function of only the dimensionless variable, $\omega = 2M_p \nu/q^2$. Since

$$\nu W_2 = \nu \frac{(d^2\sigma/d\Omega dE')}{(d\sigma/d\Omega)_{\text{Mott}}} \left[1 + \frac{2}{1+R} \left(1 + \frac{\nu^2}{q^2} \right) \tan^2 \frac{\theta}{2} \right]^{-1} ,$$

where $R = \frac{\sigma_L}{\sigma_T}$, the value of νW_2 depends on the presently unknown value of R. Nevertheless, the behavior of νW_2 can still be studied on the basis of the extreme assumptions $\sigma_L = 0$ and $\sigma_T = 0$. In Figs. 12 through 14, the experimental values of νW_2 obtained from the 6°, 10°, and 18° data are shown for these assumptions. The results in these figures indicate the following:

1. If $\sigma_L = 0$, the measurements at a fixed scattering angle but different incident electron energies appear to converge to a universal curve.

However, it should be noted that the data shown in Fig. 2c, for $\theta = 6^{\circ}$ and $E_0 = 7$ GeV, are much lower than those measured at higher incident energies and the same angle, as shown in Fig. 2a. Maybe this can be explained by their different values of q^2. The maximum value of q^2 for $E_0 = 16$ GeV and $\theta = 6^{\circ}$ is less than 2.6 $(\text{GeV/c})^2$, while the maximum value of q^2 for $E_0 = 7$ GeV and $\theta = 6^{\circ}$ is less than 0.5 $(\text{GeV/c})^2$.

2. If $\sigma_L = 0$, the data at 6° and 18° indicate a negative slope while the 10° data does not, as shown in Figs. 12a, 13, and 14. The 18° data falls off faster than the 6° data as the value of ω increases. This indicates that there is still some residual weak q^2 dependence at large values of ω.

3. If $\sigma_T = 0$, the data is less converging to a universal curve as evidenced by the 6° data shown in Fig. 12b.

There have been a number of theories developed to interpret the high energy electron scattering results. The parton model predicts a magnitude for νW_2 to within a factor of two.[27] The γ_5 field theory equates νW_2 to some power of ω.[28] The Pomeranchon exchange model leads to some constant value of νW_2.[29,30] A model based on quantum electrodynamics indicates that νW_2 should exhibit a weak q^2 dependence.[31]

At present, the most detailed predictions come from a vector dominance model.[32] In this model, the longitudinal and transverse cross sections are explicitly given, and their ratio can be expressed as

$$R = \frac{\sigma_L}{\sigma_T} = \frac{q^2}{m_\rho^2} \left(\frac{K}{\nu}\right)^2 \xi(K) \quad ,$$

where

$$\xi(K) = \frac{\sigma^{L}_{\rho P}(q^2)}{\sigma^{T}_{\rho P}(q^2)} \quad ,$$

m_ρ = mass of the ρ-meson,

$\sigma^{L}_{\rho P}$ = longitudinal ρP cross section,

and

$\sigma^{T}_{\rho P}$ = transverse ρP cross section.

At high q^2, this model predicts a large longitudinal cross section which is a very stringent condition. It has also been suggested, in view of the large range of extrapolation involved in the vector dominance theory, that one ought to treat the vector meson mass and also ξ as free parameters.[33]

Using the ρ-mass and $\xi = 1.5$, the data at 6° and 10° agree to better than 50% with the predictions if $\sigma_{\gamma p}$ is assumed to be constant. As shown in Fig. 15, the cross sections measured at 18° and 13.3 GeV are in very good agreement with the predictions given by $m_v = m_\phi$, and $\xi = 1$. Figure 16 gives a separation of σ_L and σ_T at W = 4 GeV and $q^2 = 4$ (GeV/c)^2, using the SLAC-MIT data measured at 10°, 18°, and 26°. The longitudinal cross section obtained is much smaller than that predicted by the vector dominance model.

Application of current algebra and current commutation relations led to many sum rules for electron scattering.[2,34-38] Comparison of these sum rule predictions with experimental results, evaluated with only the 6° data, are given in the following.

A. Bjorken Sum Rule[2]: $\int_{\frac{q^2}{2M_p}}^{\infty} d\nu \left[W_2^{\text{proton}} + W_2^{\text{neutron}}\right] \geq \frac{1}{2}$.

Since the neutron data is not available, a less plausible quark model argument gives

$$\int_{\frac{q^2}{2M_p}}^{\infty} W_2^{\text{proton}}\, d\nu \geq 1 ,$$

whereas $q^2 = 2\ (\text{GeV/c})^2$, the above integral was evaluated to be ~ 0.50 by assuming $\sigma_T = 0$, and the number became smaller if assuming $\sigma_L = 0$.

B. Callan and Gross Sum Rule[33]: $\sigma_T = 0$, if the electromagnetic current was made of boson field; and $\sigma_L = 0$, if fermion field.

The result shown in Fig. 16 indicates neither of these predictions is correct.

C. Gottfried Sum Rule[34]: $\int_{\frac{q^2}{2M}}^{\infty} W_2\, d\nu = 1 - \left(G_{EP}^2 + \tau G_{MP}^2\right)/(1+\tau)$, where

$\tau = q^2/4M_p^2$, and G_{EP}, G_{MP} = elastic proton form factors. For $q^2 = 1\ (\text{GeV/c})^2$, the integral is equal to ~ 0.8 for $\sigma_T = 0$, and ~ 0.7 for $\sigma_L = 0$. It can not be satisfied for ν less than 20 GeV.

It should be emphasized that most conclusions discussed in this section are based mainly upon various assumptions made for σ_L and σ_T. Some important theoretical questions can only be answered by a good separation of W_1 and W_2. Until that can be carefully done, an understanding of the voluminous experimental results can only be reached through using various parametrizations.

V. Total Photon-Proton Cross Section

The total photon-proton absorption cross section, $\sigma_{\gamma p}(K)$, has normally been measured directly in experiments using liquid hydrogen bubble chambers.[39-41]

However, through extrapolation procedures the inelastic electron scattering experiments provide an indirect method for obtaining such information since in the limit of $q^2 = 0$, the quantity $\frac{1}{\Gamma_t} \frac{d^2\sigma}{d\Omega dE'}$ should be identical to the total photoabsorption cross section. Figure 17 shows an example of the earlier attempts in making such an extrapolation for the nucleon resonances.[6] This extrapolation can best be done with the SLAC-MIT data[7] measured at 1.5^o and incident electron energies ranging from 5 to 20 GeV, as the values of q^2 for that data are smaller, extending only from 0.013 to 0.26 $(GeV/c)^2$. The radiative corrections have not been a serious problem, as the major part of the corrections to these data is simply the subtraction of the radiative tail from the elastic scattering which can be calculated very accurately with the known elastic proton form factors.[13] The results from the e-p inelastic scattering experiment at SLAC, for equivalent photon energies of up to 15 GeV, are shown in Fig. 18.[7] It should be noted that the total photoabsorption cross section exhibits a slowly decreasing trend as the photon energy increases.

VI. Axial Form Factor

Nambu and Shrauner first showed that the cross section for electroproduction at pion threshold

$$e + p \rightarrow e + p + \pi^o$$
$$\rightarrow e + n + \pi^+$$

can be expressed in terms of the elastic electromagnetic form factors and the axial vector form factor, $G_A(q^2)$, of the nucleon in the ideal soft pion limit.[1] In the absence of a precision high energy neutrino experiment, the e-p inelastic scattering experiments offer a good possibility for determining the unknown axial form factor, especially at large values of q^2. Earlier attempts along this line yielded only crude results which were inconsistent with the meager information obtained from

neutrino experiments.[42] Recently, Nambu and Yoshimura re-examined this problem.[43] Possible corrections due to pion mass, pion momentum, and modification of the PCAC condition,[44] were considered. Using the combined data from different laboratories, these authors extracted the values of $G_A(q^2)$ which covered a range of q^2 of up to 6 $(GeV/c)^2$ and fitted them by the dipole formula

$$G_A(q^2) = \frac{1.49}{\left[1 + \frac{q^2}{(1.32)^2}\right]^2} \quad .$$

This fit and the experimental data are shown in Fig. 19. For small q^2, the data intends to give the correct limit $G_A(0) = 1$, while the fit does not.

REFERENCES

1. Y. Nambu and E. Shrauner, Phys. Rev. 128, 862 (1962); S. L. Adler and F. J. Gilman, Phys. Rev. 152, 1460 (1966); Riazuddin and B. W. Lee, Phys. Rev. 146, 1202 (1966).
2. J. D. Bjorken, Phys. Rev. Letters 16, 408 (1966); and Phys. Rev. 163, 1767 (1967).
3. N. Christ and T. D. Lee, Phys. Rev. 143, 1310 (1966).
4. E. D. Bloom, D. H. Coward, H. DeStaebler, J. Drees, G. Miller, L. W. Mo, and R. E. Taylor; and M. Breidenbach, J. I. Friedman, G. C. Hartmann, and H. W. Kendall, Report No. SLAC-PUB-642, Stanford Linear Accelerator Center, Stanford, California (1969) (to be published).
5. M. Breidenbach, J. I. Friedman, H. W. Kendall; and E. D. Bloom, D. H. Coward, H. DeStaebler, J. Drees, L. W. Mo, and R. E. Taylor, Report No. SLAC-PUB-650, Stanford Linear Accelerator Center, Stanford, California (1969) (to be published).
6. W. K. H. Panofsky, Proceedings of the International Conference on High Energy Physics, Vienna, Austria (1968); p. 23. J. Prentki and J. Steinberger, Editors (CERN Scientific Information Service, Geneva, 1968).
7. E. D. Bloom, R. L. Cottrell, D. H. Coward, H. DeStaebler, Jr., J. Drees, G. Miller, L. W. Mo, R. E. Taylor; and J. I. Friedman, G. C. Hartmann, and H. W. Kendall, Report No. SLAC-PUB-653, Stanford Linear Accelerator Center, Stanford, California (1969) (to be published).
8. S. D. Drell and J. D. Walecka, Annals of Phys. 28, 18 (1964); J. D. Bjorken, unpublished; R. von Gehlen, Phys. Rev. 118, 1455 (1960); M. Gourdin, Nuovo Cimento 21, 1094 (1961).

9. The form factors are defined by

$$T_{\mu\nu} = \left(g_{\mu\nu} - \frac{q_\mu q_\nu}{q^2}\right) W_1(q^2, W)$$

$$+ \frac{1}{M_p^2}\left(P_\mu - \frac{P\cdot q}{q^2} q_\mu\right)\left(P_\nu - \frac{P\cdot q}{q^2} q_\nu\right) W_2(q^2, W)$$

where the second rank tensor $T_{\mu\nu}$ represents the hadronic contribution to the cross section; $g_{\mu\nu}$, the metric tensor; and P, the proton momentum (see Ref. 8). If the target is polarized and if the time-reversal invariance was also violated, then a third form factor, $W_3(q^2, W)$, would be required (see Ref. 3).

10. L. N. Hand, Phys. Rev. 129, 1834 (1963).

11. F. J. Gilman, Phys. Rev. 167, 1365 (1968).

12. W.K.H. Panofsky, Proceedings of the International Symposium on Electron and Photon Interactions at High Energies, Hamburg, Germany (1965) (Springer-Verlag, Berlin, Germany, 1965); R. E. Taylor, Proceedings of the International Symposium on Electron and Photon Interactions at High Energies, Stanford Linear Accelerator Center, Stanford University, Stanford, California (1967). Details on beam optics for these spectrometers can be found in Report No. SLAC-TN-65-29, by L. W. Mo and C. Peck (1965); and Report No. SLAC-TN-65-40, by L. W. Mo (1965); Stanford Linear Accelerator Center, Stanford, California (unpublished).

13. L. W. Mo and Y. S. Tsai, Rev. Mod. Phys. 41, 205 (1969).

14. J. D. Walecka and P. A. Zucker, Phys. Rev. 167, 1479 (1968).

15. P. L. Pritchett, J. D. Walecka, and P. A. Zucker, Stanford University, Stanford, California, preprint (1969), to be submitted to the Phys. Rev.

These authors pointed out that if more reasonable π-p phase-shift[16] had been used, the predicted width for the 1.512- and the 1.688-GeV resonance will be in better agreement with that given in Table 1 (private communication).

16. A. D. Brody, D.W.G.S. Leith, B. G. Levi, and B. C. Shen; and D. Herndon, R. Longacre, L. Price, A. H. Rosenfeld, and P. Söding, Phys. Rev. Letters 22, 1401 (1969).

17. A. J. Dufner and Y. S. Tsai, Phys. Rev. 168, 1801 (1968).

18. W. Bartel, B. Dudelzak, H. Krehbiel, J. McElroy, U. Meyer-Berkhout, W. Schmidt, V. Walther, and G. Weber, Phys. Letters 28B, 148 (1968).

19. A. A. Cone, K. W. Chen, J. R. Dunning, G. Hartwig, N. F. Ramsey, J. K. Walker, and R. Wilson, Phys. Rev. 156, 1490 (1967).

20. H. L. Lynch, J. V. Allaby, and D. M. Ritson, Phys. Rev. 169, 1635 (1967).

21. W. Bartel, B. Dudelzak, M. Krehbiel, J. McElroy, U. Meyer-Berkhout, W. Schmidt, V. Walther, and G. Weber, Phys. Letters 27B, 660 (1968).

22. F. W. Brasse, J. Engler, E. Ganszauge, and M. Schweizer, DESY Report No. 67/34 (1967).

23. W. Albrecht, F. W. Brasse, H. Dorner, W. Flauger, K. Frank, J. Gayler, H. Hultschig, J. May, and E. Ganszauge, Phys. Letters 28B, 225 (1968); also DESY Report No. 69/7 (1969).

24. J. D. Bjorken, Proceedings of International School of Physics "Enrico Fermi," Course 41, edited by J. Steinberger (Academic Press, Inc., New York, 1969).

25. J. D. Bjorken, Report No. SLAC-PUB-571, Stanford Linear Accelerator Center, Stanford, California (1969) (unpublished).

26. J. D. Bjorken, Phys. Rev. 179, 1547 (1969).

27. J. D. Bjorken and E. A. Paschos, Report No. SLAC-PUB-572, Stanford Linear Accelerator Center, Stanford, California (1969) (to be published).

28. S. J. Drell, D. J. Levy, and T. M. Yan, Phys. Rev. Letters 22, 744 (1969).

29. H. Harari, Phys. Rev. Letters 22, 1078 (1969).

30. H. D. Abarbanel, M. L. Goldberger, and S. B. Treiman, Phys. Rev. Letters 22, 500 (1969).

31. H. Cheng and T. T. Wu, Phys. Rev. Letters 22, 1409 (1969).

32. J. J. Sakurai, Phys. Rev. Letters 22, 981 (1969).

33. C. F. Cho, G. J. Gounaris, and J. J. Sakurai, Report No. EFI-69-54, The University of Chicago, Chicago, Illinois, preprint (1969) (to be published).

34. J. M. Cornwall and R. E. Norton, Phys. Rev. 177, 2584 (1969).

35. C. G. Callan, Jr., and D. J. Gross, Phys. Rev. Letters 21, 311 (1968); and Phys. Rev. Letters 22, 156 (1969).

36. K. Gottfried, Phys. Rev. Letters 18, 1174 (1967).

37. S. L. Adler and Wu-ki Tung, Phys. Rev. Letters 22, 978 (1969).

38. R. Jackiw and G. Preparata, Phys. Rev. Letters 22, 975 (1969).

39. SLAC-Tufts-UCB/LRL Collaboration, Report No. SLAC-PUB-618, Stanford Linear Accelerator Center, Stanford, California (1969) (to be published).

40. J. Ballam, G. B. Chadwick, Z.G.T. Guiragossián, P. Klein, A. Levy, M. Menke, E. Pickup, P. Seyboth, T. H. Tan, and G. Wolf, Phys. Rev. Letters 21, 1544 (1968).

41. Aachen-Berlin-Bonn-Hamburg-Heidelberg-München Collaboration, Phys. Rev. 175, 1669 (1968).

42. A. H. Gleeson, M. G. Gundzik, and J. G. Kuriyan, Phys. Rev. 173, 1708 (1968).

43. Y. Nambu and M. Yoshimura, Report No. EFI-69-81, The University of Chicago, Chicago, Illinois preprint (1969) (to be published).

44. S. L. Adler, Phys. Rev. 177, 2426 (1969).

TABLE I

PRELIMINARY RESULTS ON THE RESONANCES

E	θ	$\frac{d\sigma}{d\Omega}$ (cm^2/sr)		
		N_1^*	N_2^*	N_3^*
		M = 1.219 ± 0.010 GeV	M = 1.503 ± 0.010 GeV	M = 1.691 ± 0.010 GeV
		Γ = 0.130 ± 0.015 GeV	Γ = 0.077 ± 0.015 GeV	Γ = 0.102 ± 0.010 GeV
(GeV)	(Degree)			
7.00	6.0	$(2.15 \pm 0.17) \times 10^{-30}$	$(5.21 \pm 0.37) \times 10^{-31}$	$(5.30 \pm 0.29) \times 10^{-31}$
10.00	6.0	$(3.95 \pm 0.25) \times 10^{-31}$	$(1.36 \pm 0.12) \times 10^{-31}$	$(1.48 \pm 0.16) \times 10^{-31}$
13.50	6.0	$(7.02 \pm 0.84) \times 10^{-32}$	$(3.62 \pm 0.40) \times 10^{-32}$	$(4.17 \pm 0.83) \times 10^{-32}$
16.02	6.0	$(1.24 \pm 0.19) \times 10^{-32}$	$(9.81 \pm 1.41) \times 10^{-33}$	$(1.43 \pm 0.42) \times 10^{-32}$

FIGURE CAPTIONS

1. Schematic diagram illustrating where the cross section must be known in order to make the radiative corrections to a cross section measured at point c.
2. Three radiatively corrected e-p inelastic scattering spectra measured at:
   a. $\theta = 6^{\circ}$, $E_0 = 7$ GeV ($0.2 \leq q^2 \leq 0.5$ (GeV/c)^2);
   b. $\theta = 6^{\circ}$, $E_0 = 16$ GeV ($0.7 \leq q^2 \leq 2.6$ (GeV/c)^2); and
   c. $\theta = 10^{\circ}$, $E_0 = 17.7$ GeV ($1.6 \leq q^2 \leq 7.3$ (GeV/c)^2).
3. Radiatively corrected spectra measured at $\theta = 18^{\circ}$ and various incident electron energies. For the sake of clarity, only hand-drawn curves passing through the measured data are shown. The typical statistical errors are indicated by the few data points shown.
4. The e-p inelastic scattering spectrum, measured at $\theta = 6^{\circ}$ and $E_0 = 7$ GeV, resolved into four Breit-Wigner peaks and a polynomial background by a numerical fitting procedure.
5. The cross section ratio ($\sigma_{\text{resonance}}/\sigma_{\text{elastic}}$) for N*(1238).
6. The cross section ratio ($\sigma_{\text{resonance}}/\sigma_{\text{elastic}}$) for N*(1512).
7. The cross section ratio ($\sigma_{\text{resonance}}/\sigma_{\text{elastic}}$) for N*(1688).
8. The separated inelastic proton form factors W_1 and W_2 at $q^2 = 0.773$ (GeV/c)^2 according to the measurements of Albrecht et al.
9. The separated inelastic proton form factors W_1 and W_2 at $q^2 = 1.935$ (GeV/c)^2 according to the measurements of Albrecht et al.
10. The longitudinal cross section σ_L of the (33) resonance.
11. $(d^2\sigma/d\Omega dE')/\sigma_{\text{MOTT}}$ vs q^2 for W = 2, 3, and 3.5 GeV as measured at 10°. For elastic scattering, the ratio plotted is $(d\sigma/d\Omega)/\sigma_{\text{MOTT}}$ calculated with $\theta = 10^{\circ}$ and the dipole form factors of the proton.

12. νW_2 vs $2M_p\nu/q^2$ for data measured at 6^o. The values of W_2 were obtained by various assumptions made upon σ_T and σ_L.

13. νW_2 vs $2M_p\nu/q^2$ for data measured at 10^o. The values of W_2 were obtained by the assumption $\sigma_L = 0$.

14. νW_2 vs $2M_p\nu/q^2$ for data measured at 18^o. The values of W_2 were obtained by the assumption $\sigma_L = 0$. These results are preliminary.

15. Inelastic e-p scattering spectrum measured at $\theta = 18^o$ and $E_0 = 13.3$ GeV as compared to the predictions of Sakurai's vector dominance model.

16. Preliminary separation result made at $q^2 = 4$ $(GeV/c)^2$ and $W = 4$ GeV as compared to the predictions of Sakurai's vector dominance model.

17. Plots of $(d^2\sigma/d\Omega dE')/\Gamma_t$ for the first four resonances.

18. The total photoabsorption cross section of proton as obtained by extrapolating the e-p inelastic scattering cross sections to the limit of $q^2 \longrightarrow 0$.

19. The axial form factor as calculated by Nambu et al. using electroproduction data at pion threshold from different laboratories. The curves are numerical fits.

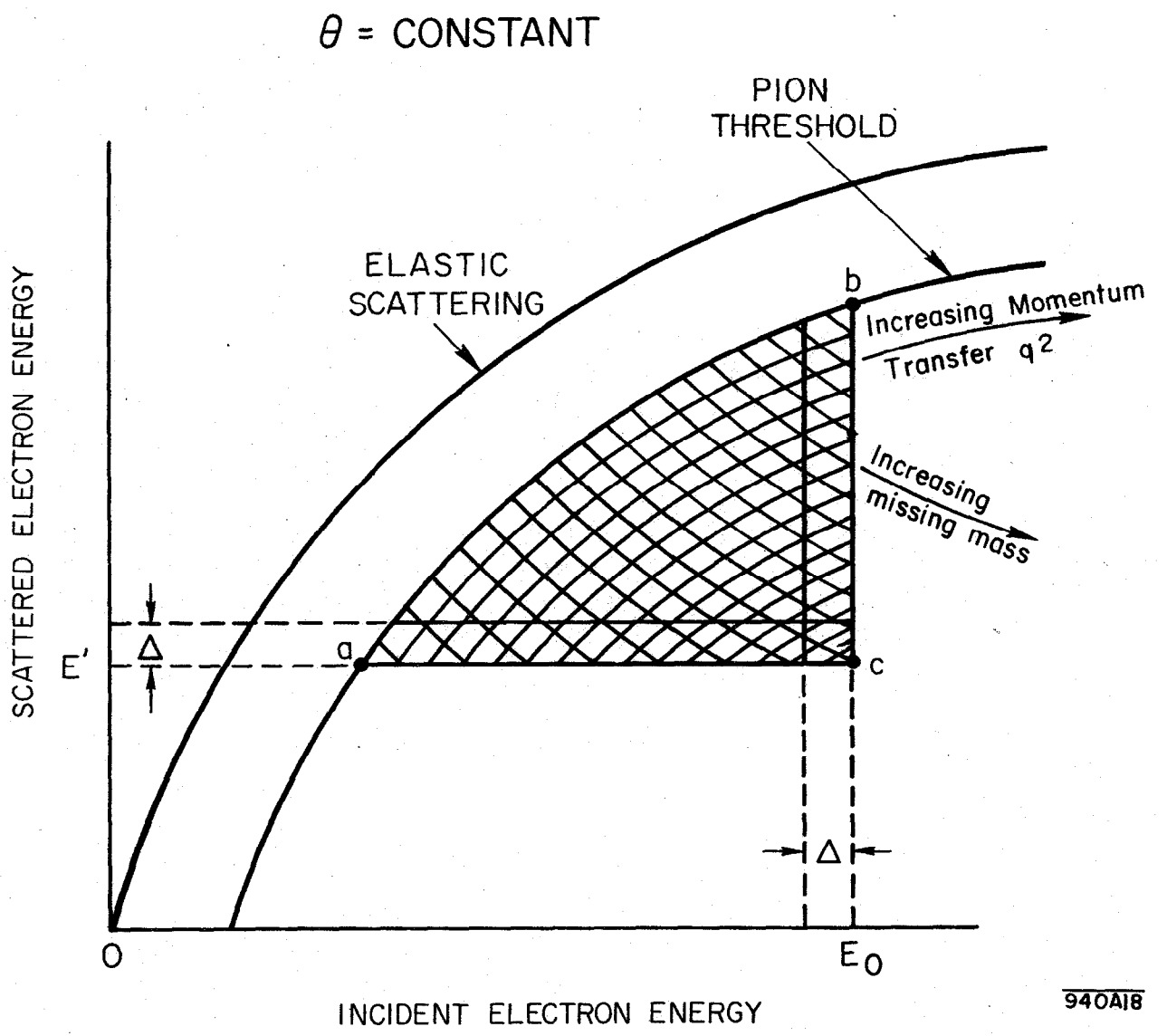
θ = CONSTANT
PION
THRESHOLD
ELASTIC
SCATTERING
b
Increasing Momentum
Transfer q²
Increasing
missing mass
SCATTERED ELECTRON ENERGY
E'
Δ
a
c
Δ
0
E0
INCIDENT ELECTRON ENERGY
940A18

Fig. 1

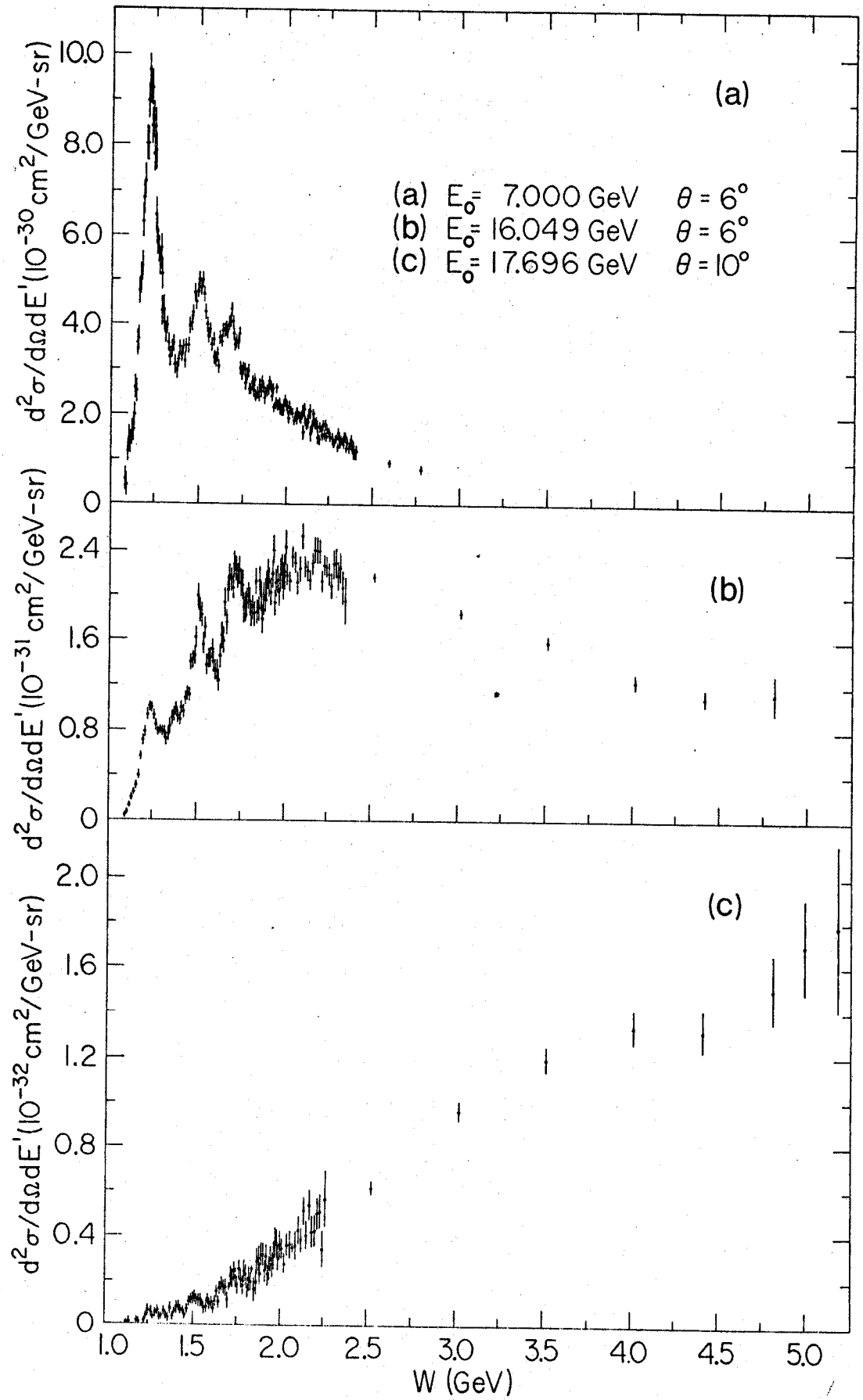
(a)
(a) E_0= 7.000 GeV θ = 6°
(b) E_0= 16.049 GeV θ = 6°
(c) E_0= 17.696 GeV θ = 10°
$d^2\sigma/d\Omega dE'(10^{-30}\,cm^2/GeV\text{-}sr)$
(b)
$d^2\sigma/d\Omega dE'(10^{-31}\,cm^2/GeV\text{-}sr)$
(c)
$d^2\sigma/d\Omega dE'(10^{-32}\,cm^2/GeV\text{-}sr)$
W (GeV)

Fig. 2

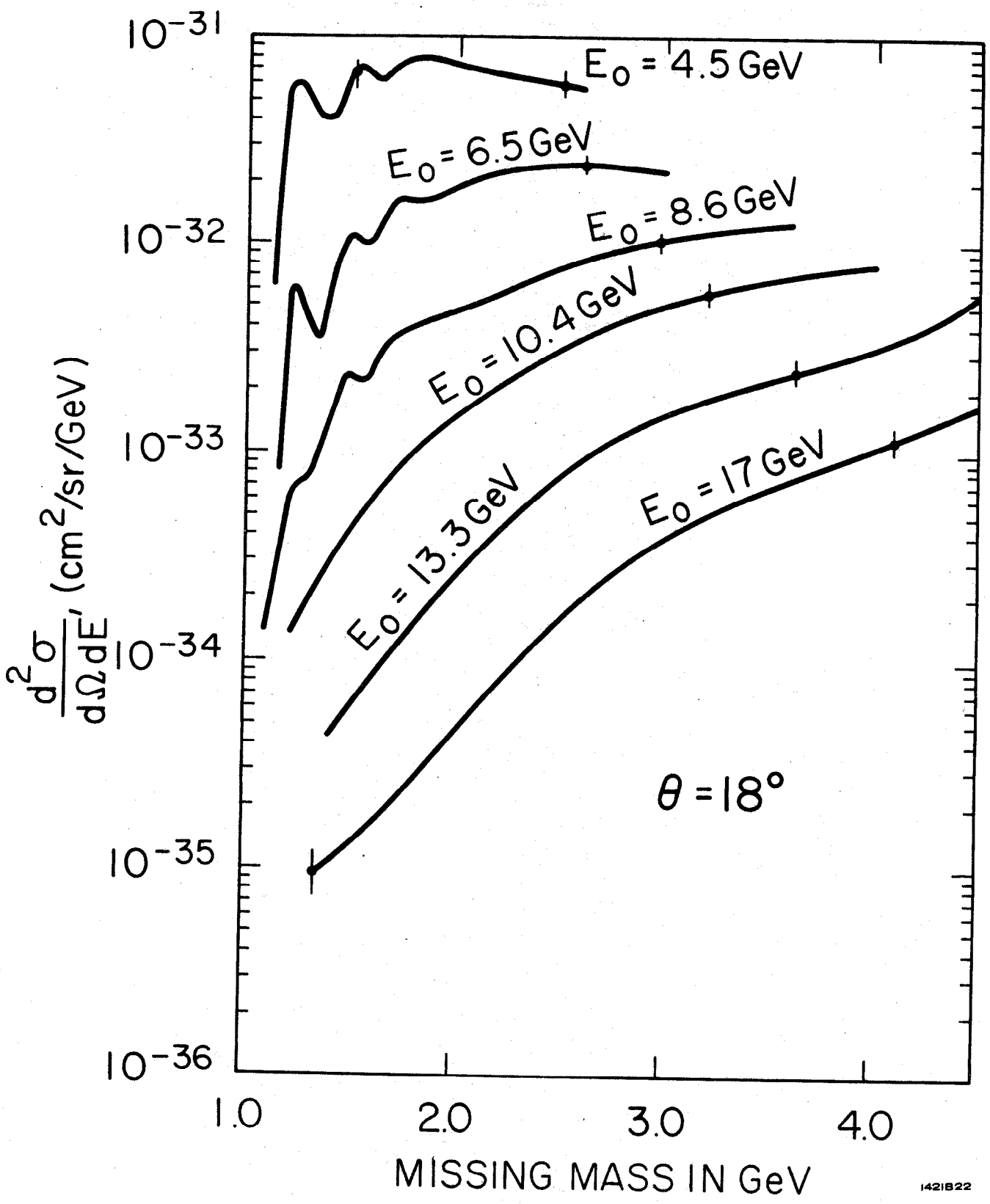
10^{-31}
10^{-32}
10^{-33}
10^{-34}
10^{-35}
10^{-36}
$\frac{d^2\sigma}{d\Omega dE'}$ (cm^2/sr/GeV)
$E_0 = 4.5$ GeV
$E_0 = 6.5$ GeV
$E_0 = 8.6$ GeV
$E_0 = 10.4$ GeV
$E_0 = 13.3$ GeV
$E_0 = 17$ GeV
$\theta = 18°$
1.0
2.0
3.0
4.0
MISSING MASS IN GeV
1421822

Fig. 3

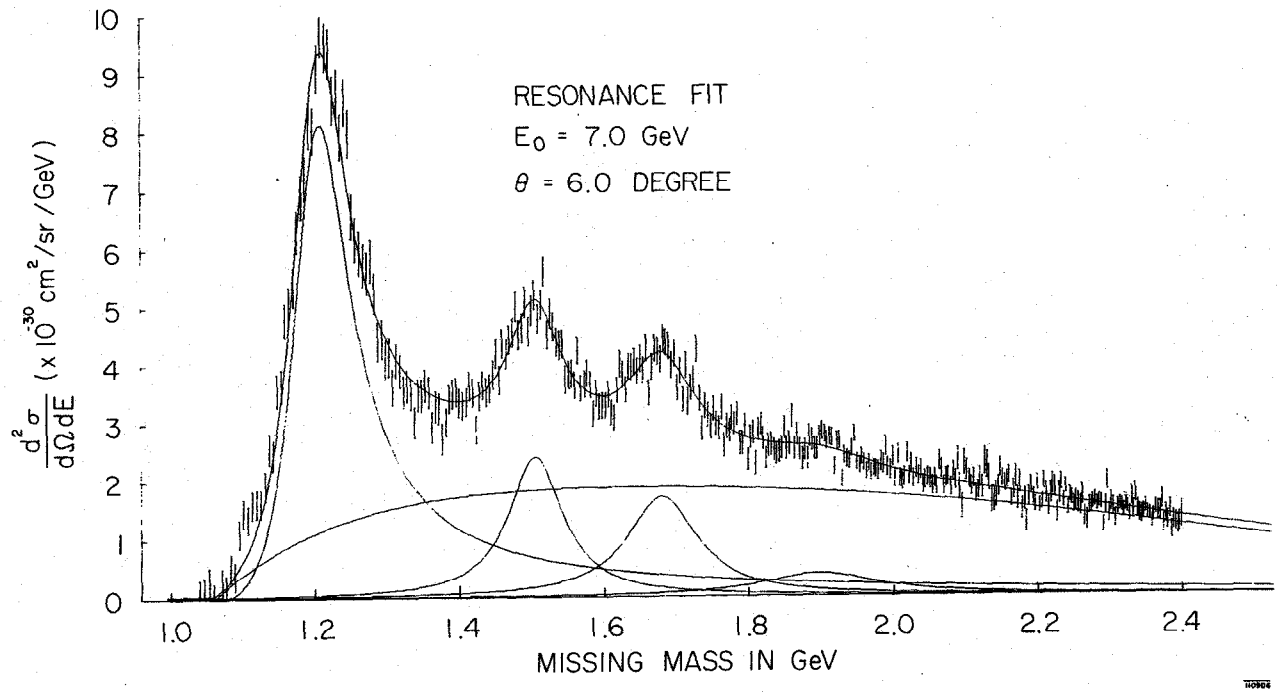
RESONANCE FIT
E_0 = 7.0 GeV
θ = 6.0 DEGREE
$\frac{d^2\sigma}{d\Omega dE}$ (x 10^{-30} cm^2/sr/GeV)
MISSING MASS IN GeV
0
1
2
3
4
5
6
7
8
9
10
1.0
1.2
1.4
1.6
1.8
2.0
2.2
2.4

Fig. 4

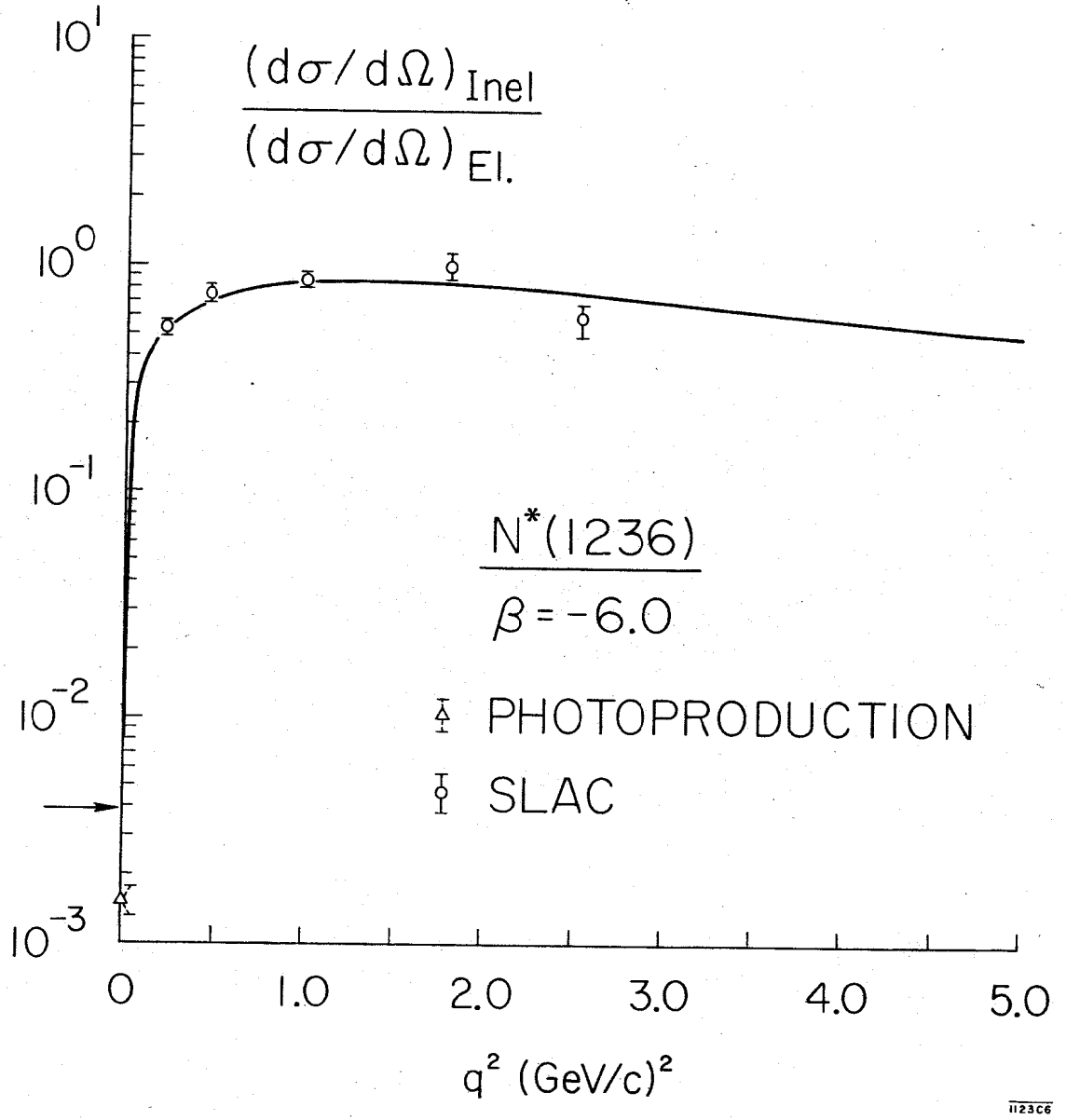
10^1
10^0
10^{-1}
10^{-2}
10^{-3}
$(d\sigma/d\Omega)_{Inel}$
$(d\sigma/d\Omega)_{El.}$
N*(1236)
β = -6.0
PHOTOPRODUCTION
SLAC
0
1.0
2.0
3.0
4.0
5.0
q^2 (GeV/c)^2
1123C6

Fig. 5

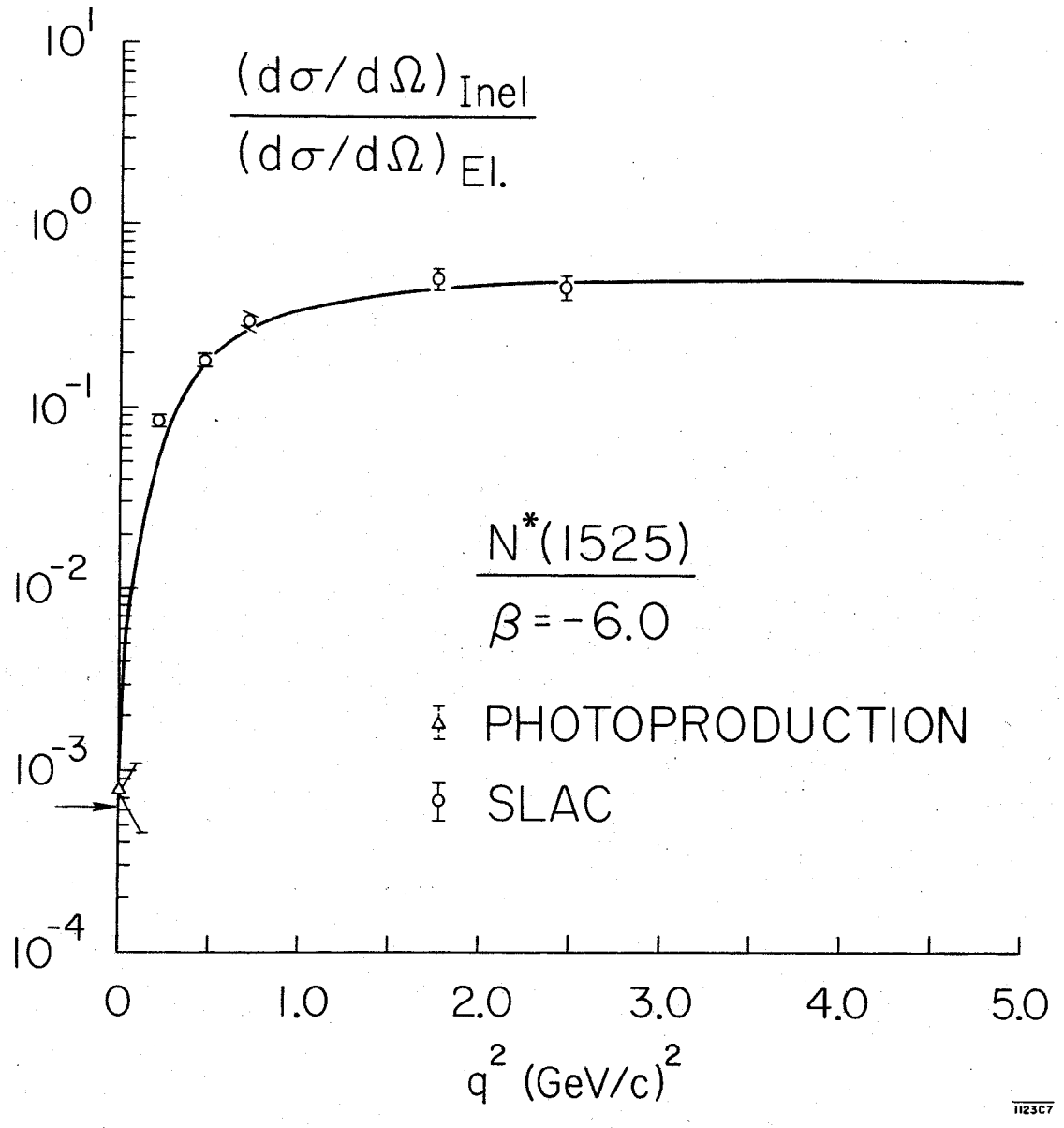
10^{1}
10^{0}
10^{-1}
10^{-2}
10^{-3}
10^{-4}
$\frac{(d\sigma/d\Omega)_{Inel}}{(d\sigma/d\Omega)_{El.}}$
$N^{*}(1525)$
$\beta = -6.0$
PHOTOPRODUCTION
SLAC
0
1.0
2.0
3.0
4.0
5.0
q^2 (GeV/c)^2
1123C7

Fig. 6

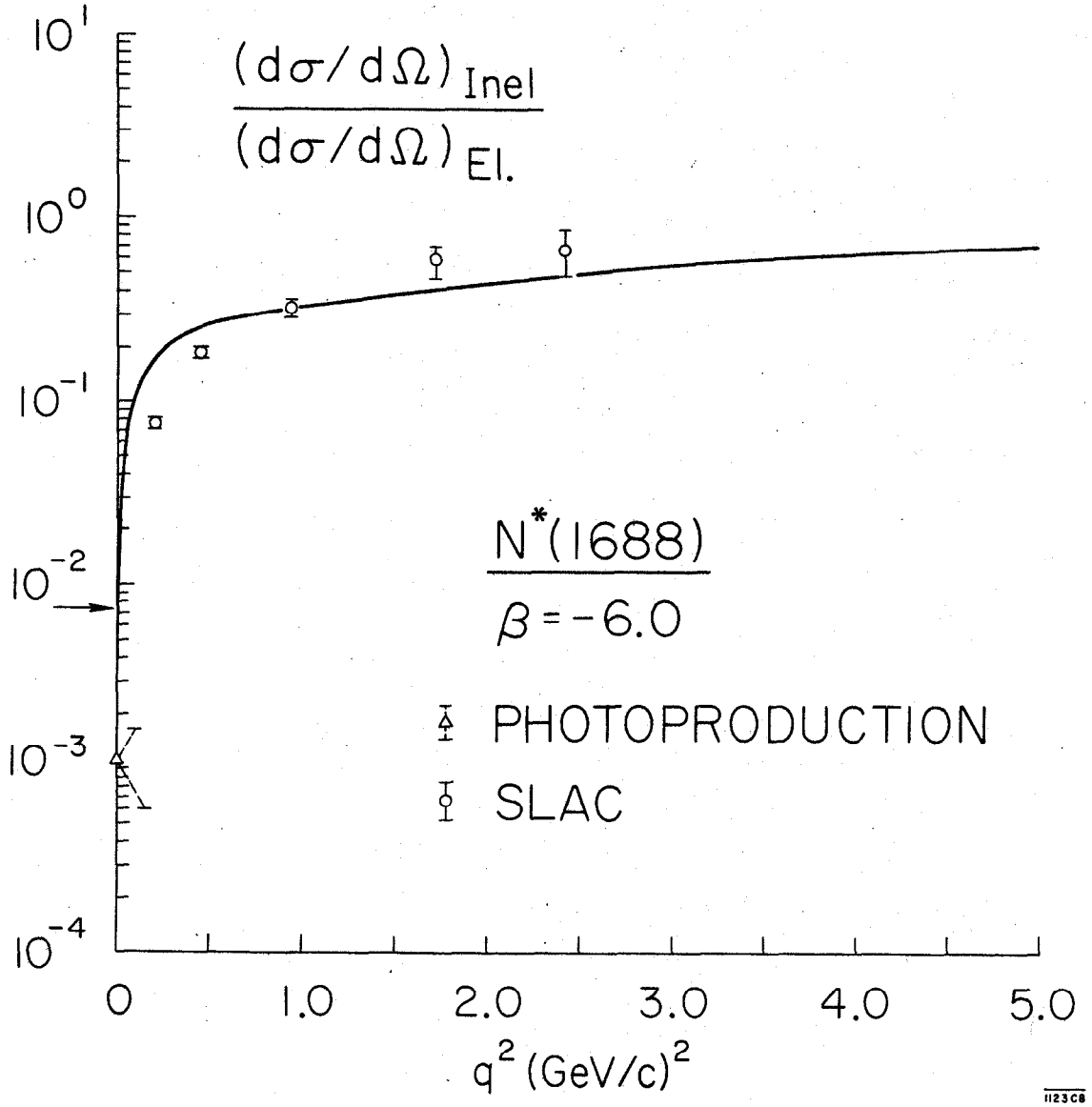
10^{1}
10^{0}
10^{-1}
10^{-2}
10^{-3}
10^{-4}
$\frac{(d\sigma/d\Omega)_{Inel}}{(d\sigma/d\Omega)_{El.}}$
$\frac{N^{*}(1688)}{\beta = -6.0}$
PHOTOPRODUCTION
SLAC
0
1.0
2.0
3.0
4.0
5.0
q^2 (GeV/c)^2
1123C8

Fig. 7

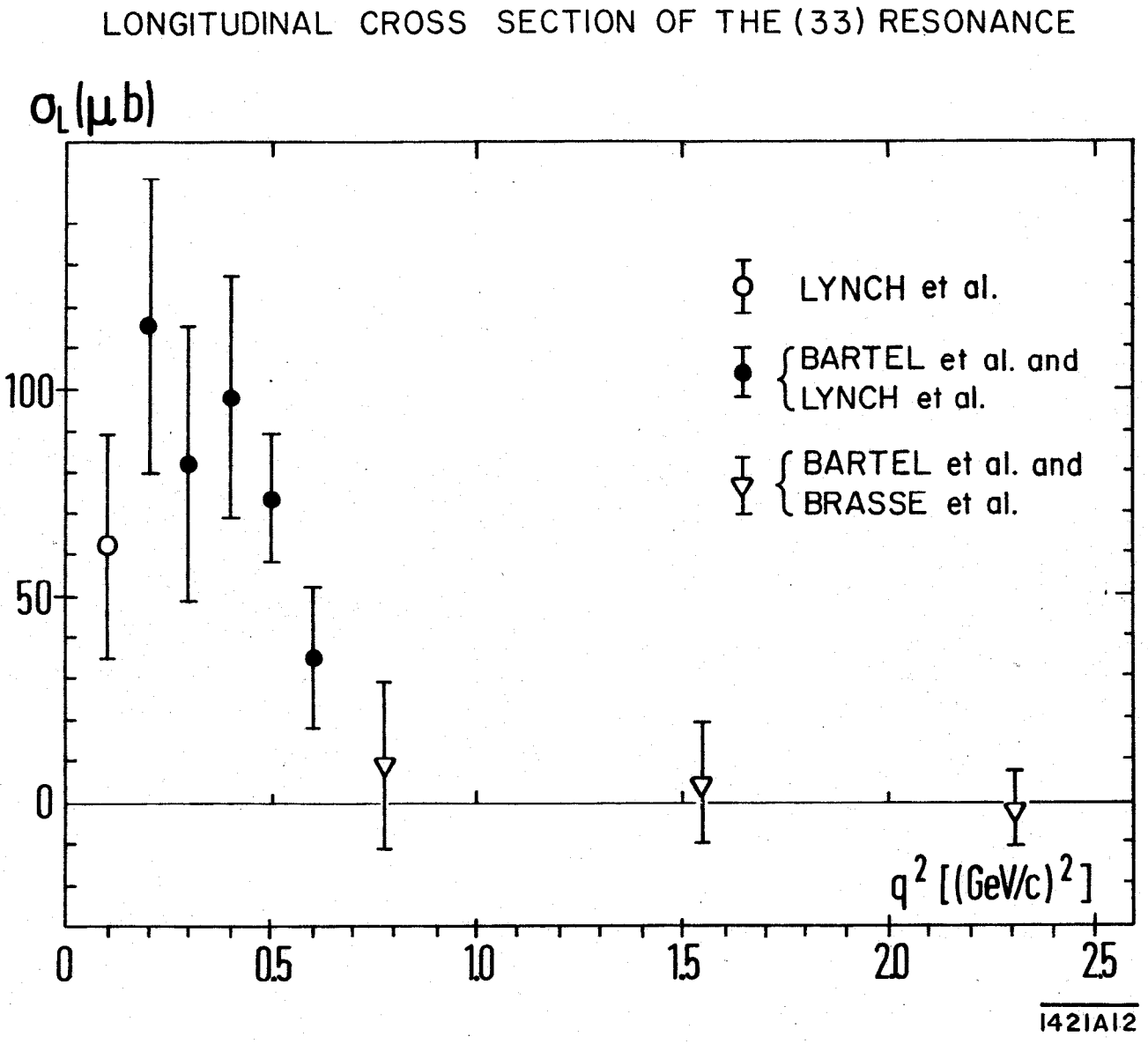
LONGITUDINAL CROSS SECTION OF THE (33) RESONANCE
σ_L (μb)
100
50
0
0
0.5
1.0
1.5
2.0
2.5
q^2 [(GeV/c)^2]
LYNCH et al.
BARTEL et al. and LYNCH et al.
BARTEL et al. and BRASSE et al.
1421A12

Fig. 8

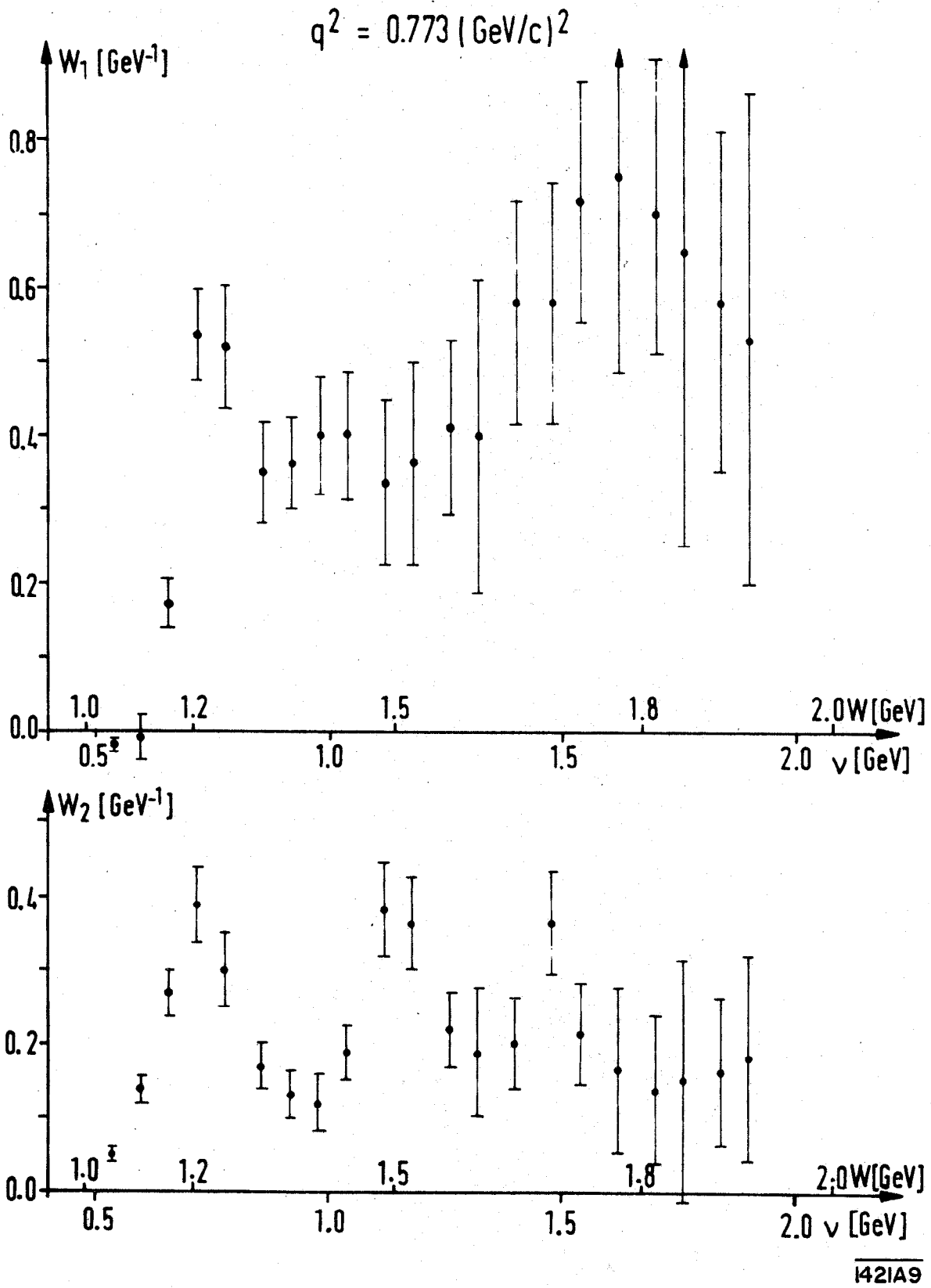
$q^2 = 0.773\ (\mathrm{GeV/c})^2$
$W_1\ [\mathrm{GeV}^{-1}]$
0.8
0.6
0.4
0.2
0.0
1.0
1.2
1.5
1.8
2.0 W[GeV]
0.5
1.0
1.5
2.0 ν [GeV]
$W_2\ [\mathrm{GeV}^{-1}]$
0.4
0.2
0.0
1.0
1.2
1.5
1.8
2.0 W[GeV]
0.5
1.0
1.5
2.0 ν [GeV]
I421A9

Fig. 9

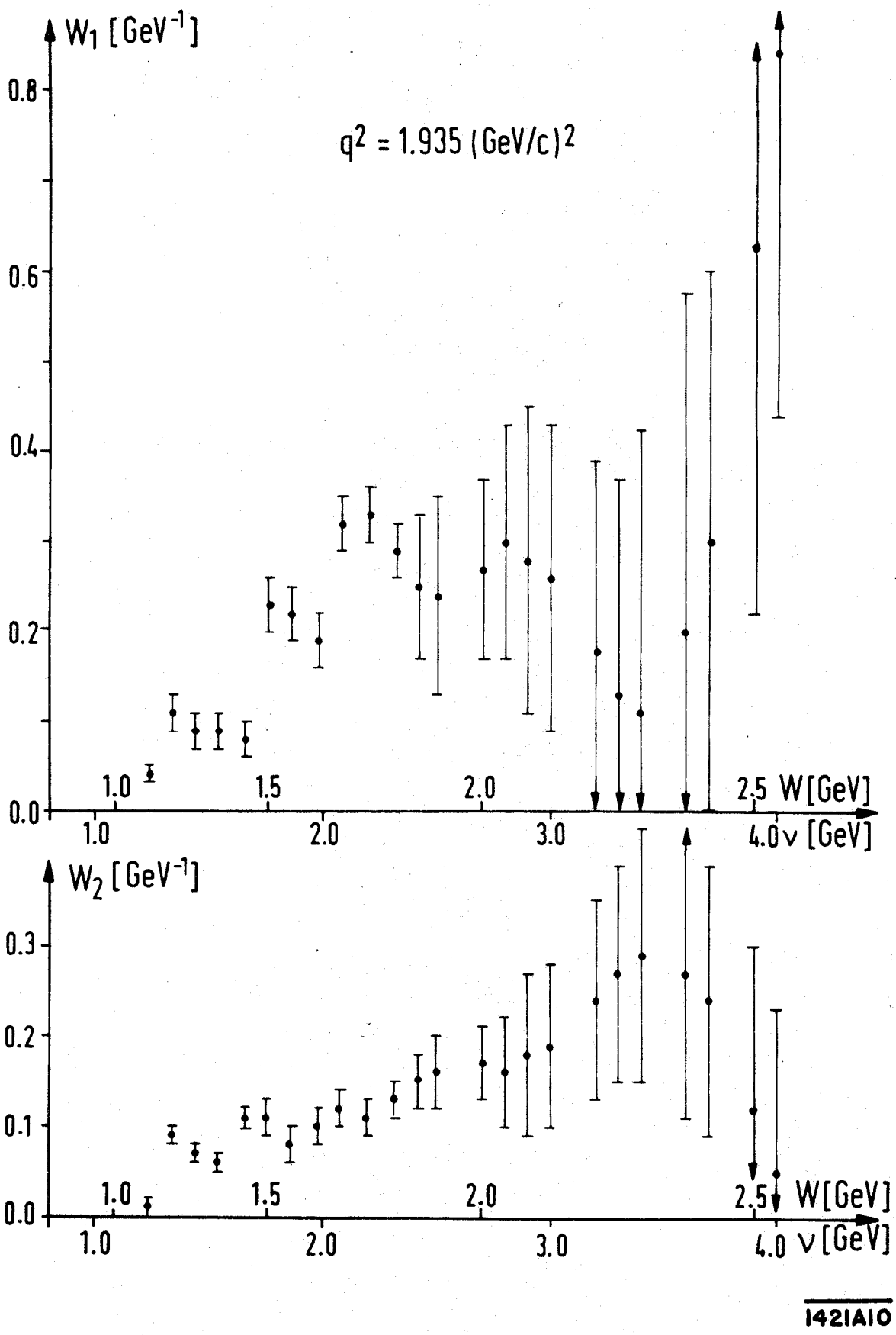
W1 [GeV-1]
q2 = 1.935 (GeV/c)2
0.8
0.6
0.4
0.2
0.0
1.0
1.5
2.0
2.5 W[GeV]
1.0
2.0
3.0
4.0 ν [GeV]
W2 [GeV-1]
0.3
0.2
0.1
0.0
1.0
1.5
2.0
2.5 W[GeV]
1.0
2.0
3.0
4.0 ν [GeV]
1421A10

Fig. 10

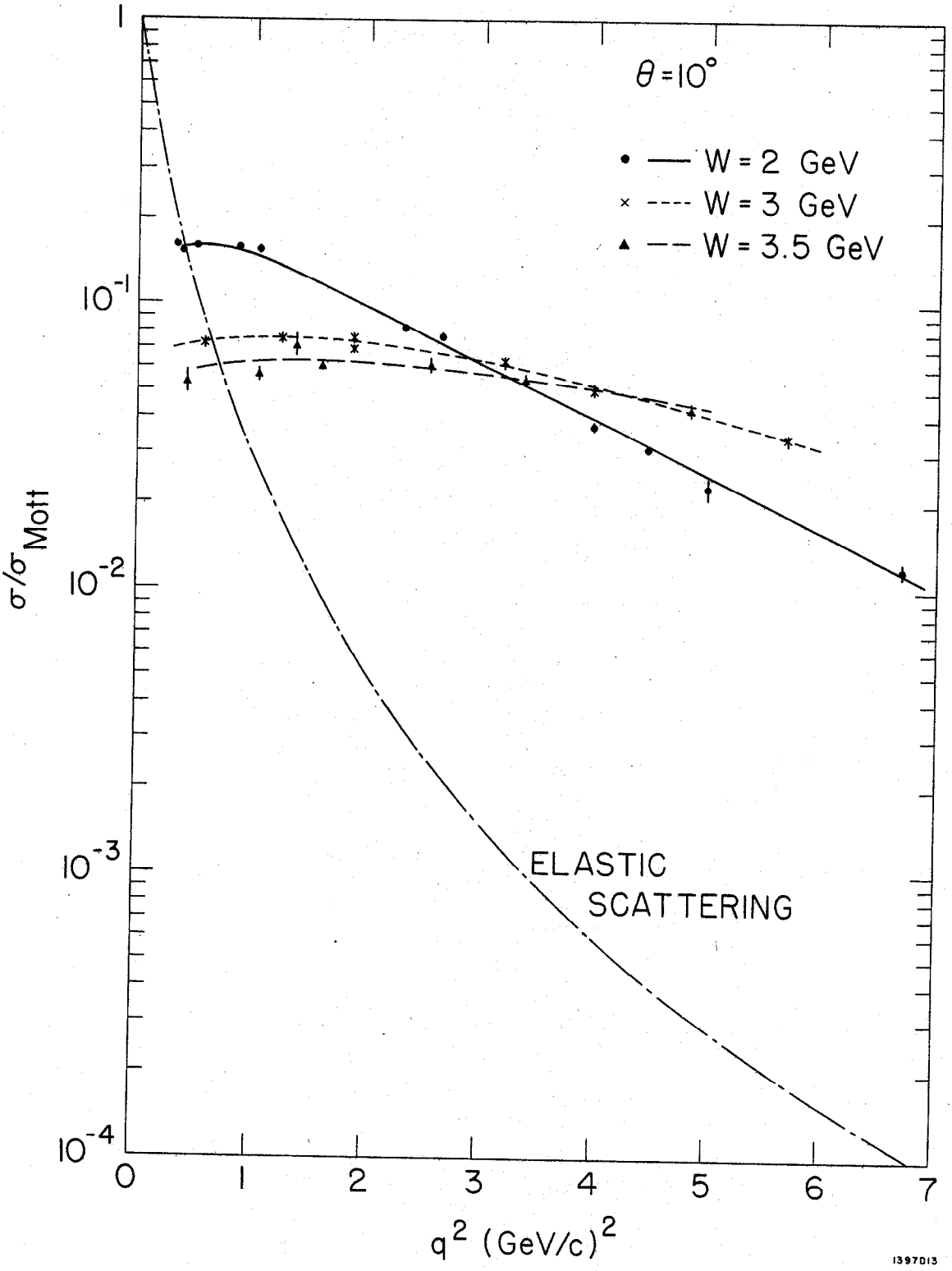
θ = 10°
W = 2 GeV
W = 3 GeV
W = 3.5 GeV
ELASTIC
SCATTERING
σ/σ Mott
q² (GeV/c)²
1
10⁻¹
10⁻²
10⁻³
10⁻⁴
0
1
2
3
4
5
6
7
1397013

Fig. 11

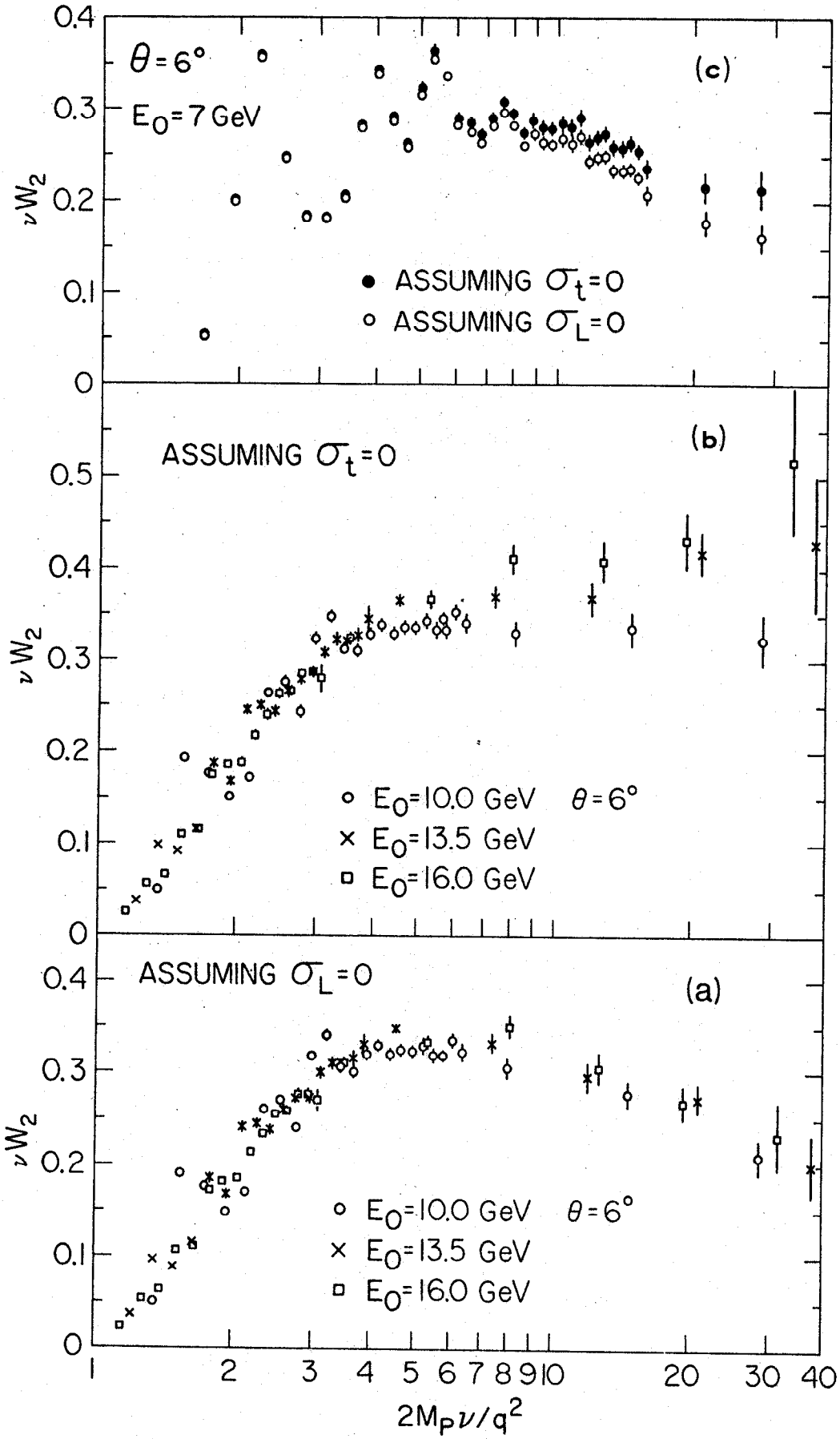
θ = 6°
E0 = 7 GeV
(c)
ASSUMING σt = 0
ASSUMING σL = 0
νW2
(b)
ASSUMING σt = 0
E0 = 10.0 GeV θ = 6°
E0 = 13.5 GeV
E0 = 16.0 GeV
(a)
ASSUMING σL = 0
E0 = 10.0 GeV θ = 6°
E0 = 13.5 GeV
E0 = 16.0 GeV
2MPν/q2

Fig. 12

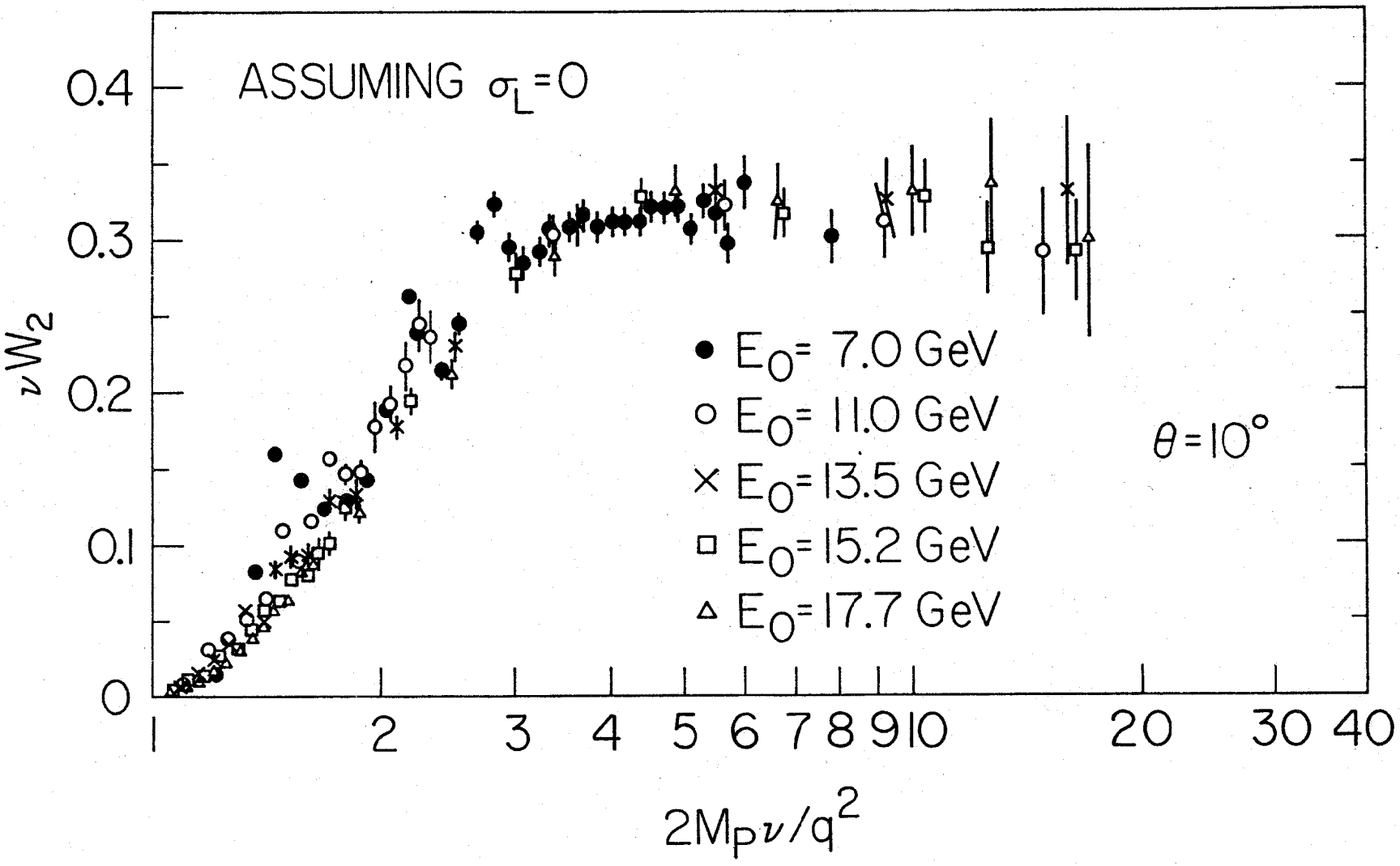
ASSUMING $\sigma_L = 0$
νW_2
0.4
0.3
0.2
0.1
0
1
2
3
4
5
6
7
8
9
10
20
30
40
$2M_P\nu/q^2$
E_0= 7.0 GeV
E_0= 11.0 GeV
E_0=13.5 GeV
E_0=15.2 GeV
E_0=17.7 GeV
θ=10°

Fig. 13

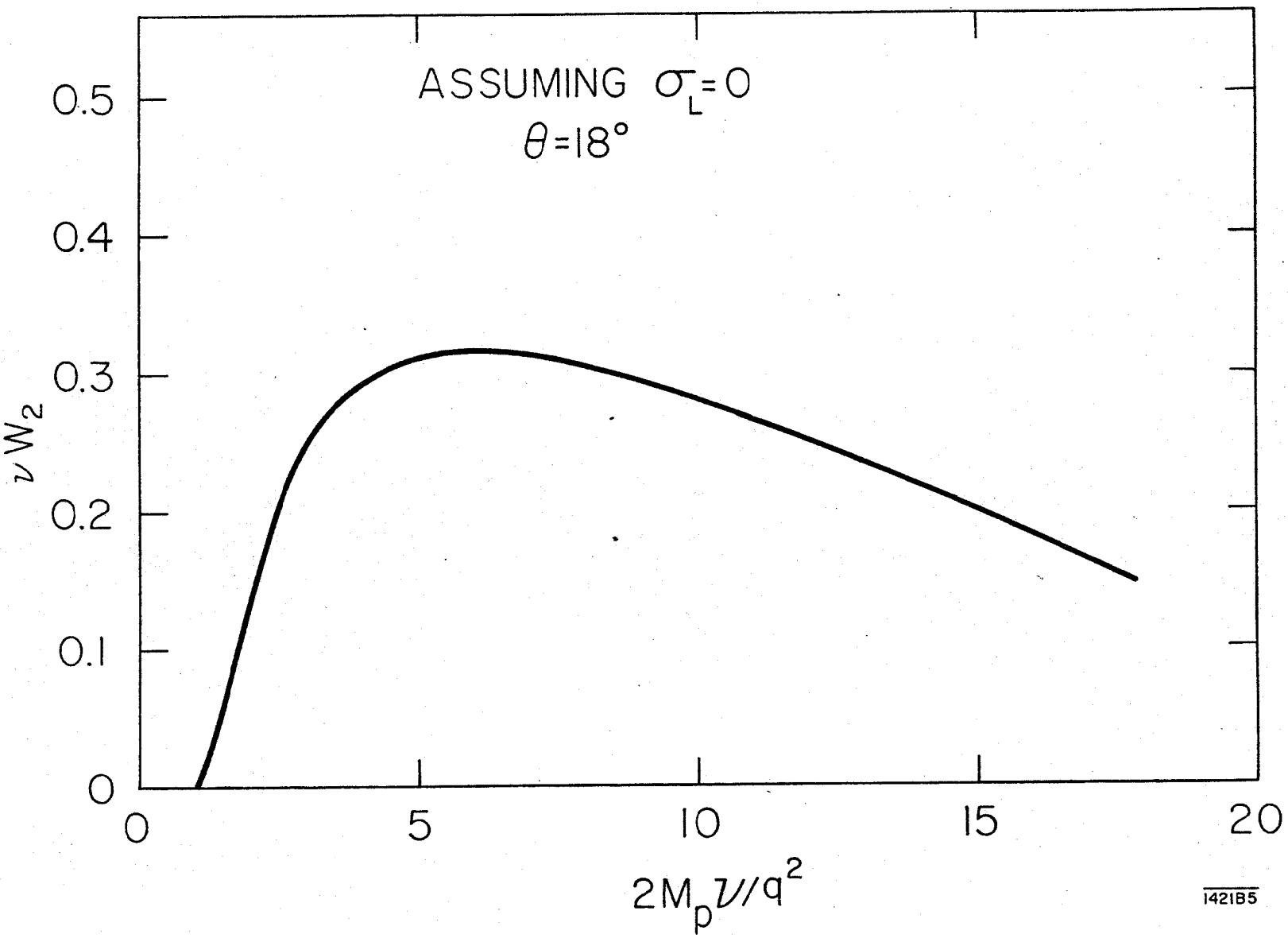
ASSUMING $\sigma_L = 0$
$\theta = 18°$
0.5
0.4
0.3
0.2
0.1
0
νW_2
0
5
10
15
20
$2M_p\nu/q^2$
1421B5

Fig. 14

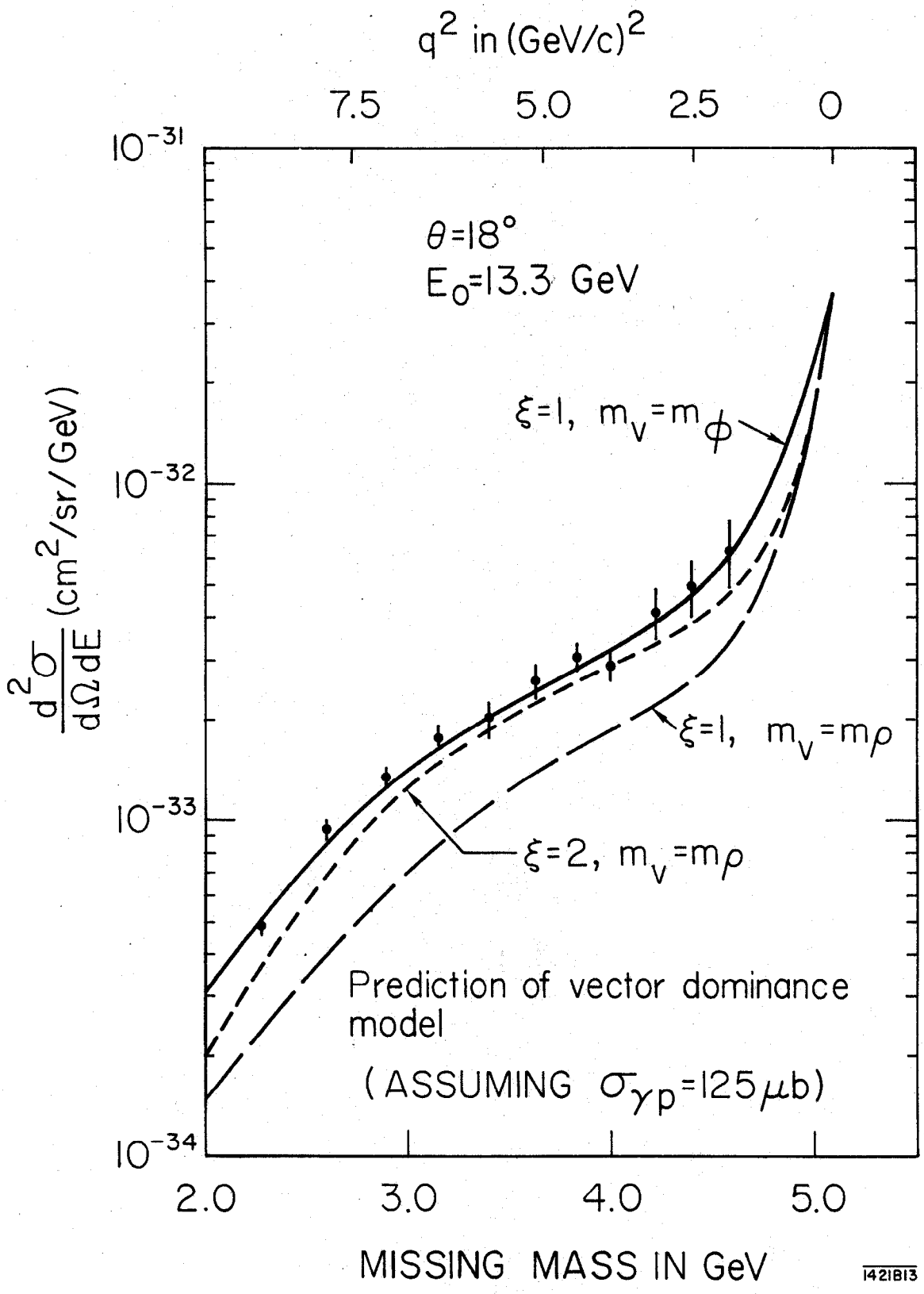
q^2 in $(GeV/c)^2$
7.5
5.0
2.5
0
10^{-31}
10^{-32}
10^{-33}
10^{-34}
θ=18°
E_0=13.3 GeV
ξ=1, $m_V=m_\phi$
ξ=1, $m_V=m_\rho$
ξ=2, $m_V=m_\rho$
Prediction of vector dominance model
(ASSUMING $\sigma_{\gamma p}$=125μb)
$\frac{d^2\sigma}{d\Omega dE}$ (cm^2/sr/GeV)
2.0
3.0
4.0
5.0
MISSING MASS IN GeV
1421813

Fig. 15

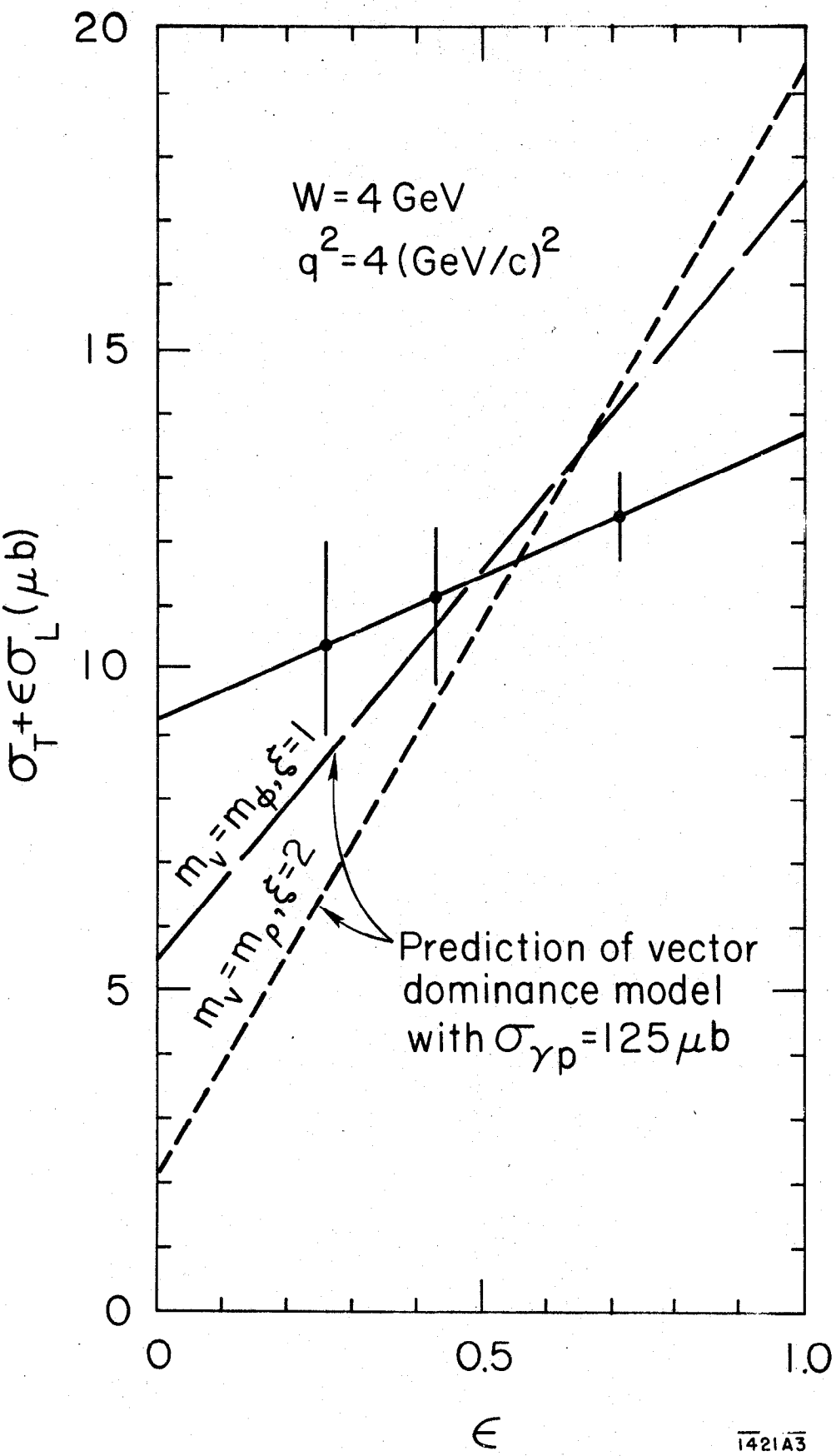
20
15
10
5
0
0
0.5
1.0
ϵ
$\sigma_T + \epsilon\sigma_L$ (μb)
W = 4 GeV
$q^2 = 4$ (GeV/c)^2
$m_V = m_\phi, \xi = 1$
$m_V = m_\rho, \xi = 2$
Prediction of vector dominance model with $\sigma_{\gamma p} = 125\,\mu$b
1421A3

Fig. 16

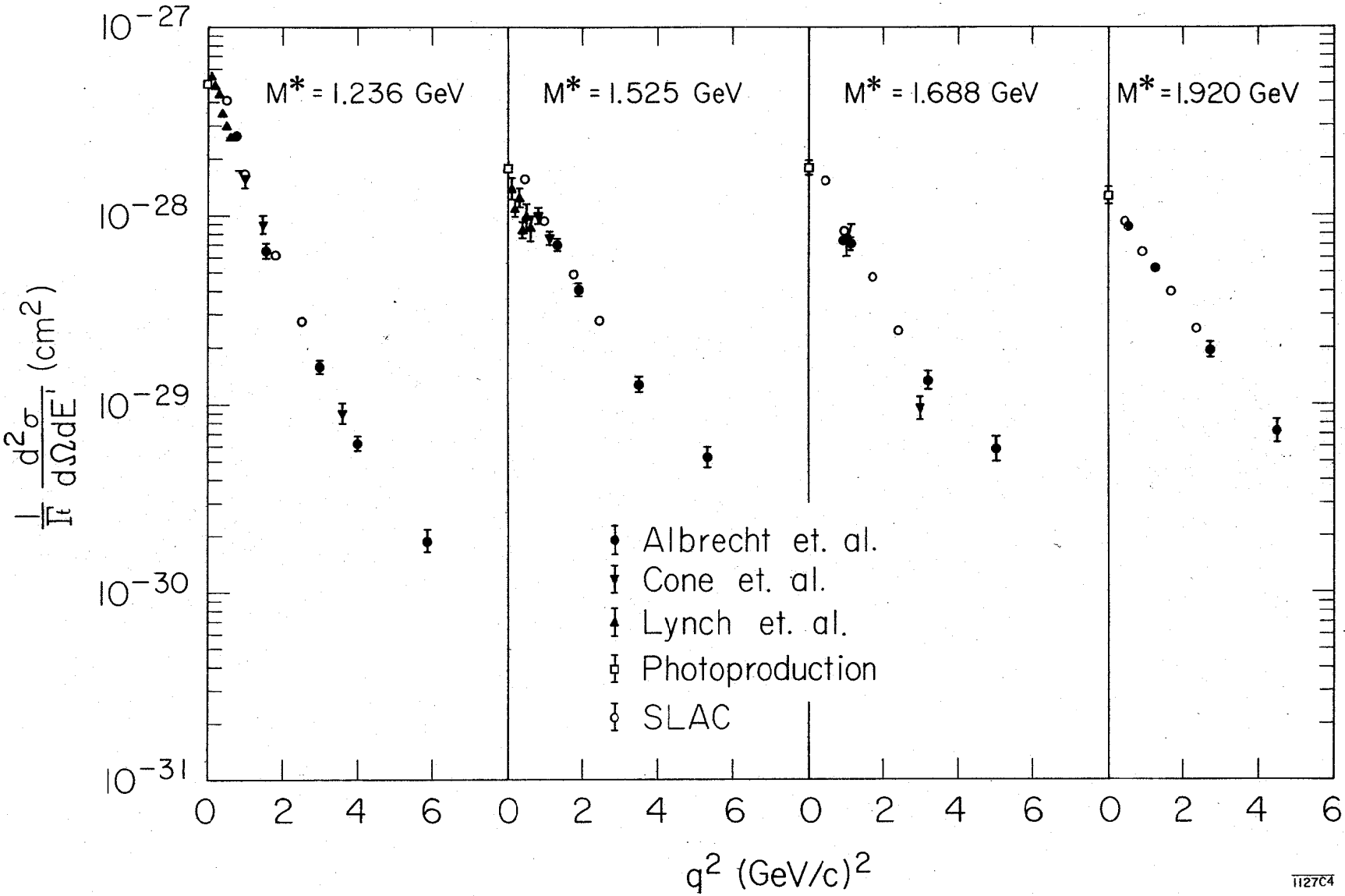
10^{-27}
10^{-28}
10^{-29}
10^{-30}
10^{-31}
$\frac{1}{\Gamma_t}\frac{d^2\sigma}{d\Omega dE'}$ (cm^2)
M* = 1.236 GeV
M* = 1.525 GeV
M* = 1.688 GeV
M* = 1.920 GeV
Albrecht et. al.
Cone et. al.
Lynch et. al.
Photoproduction
SLAC
0 2 4 6 0 2 4 6 0 2 4 6 0 2 4 6
q^2 (GeV/c)^2
1127C4

Fig. 17

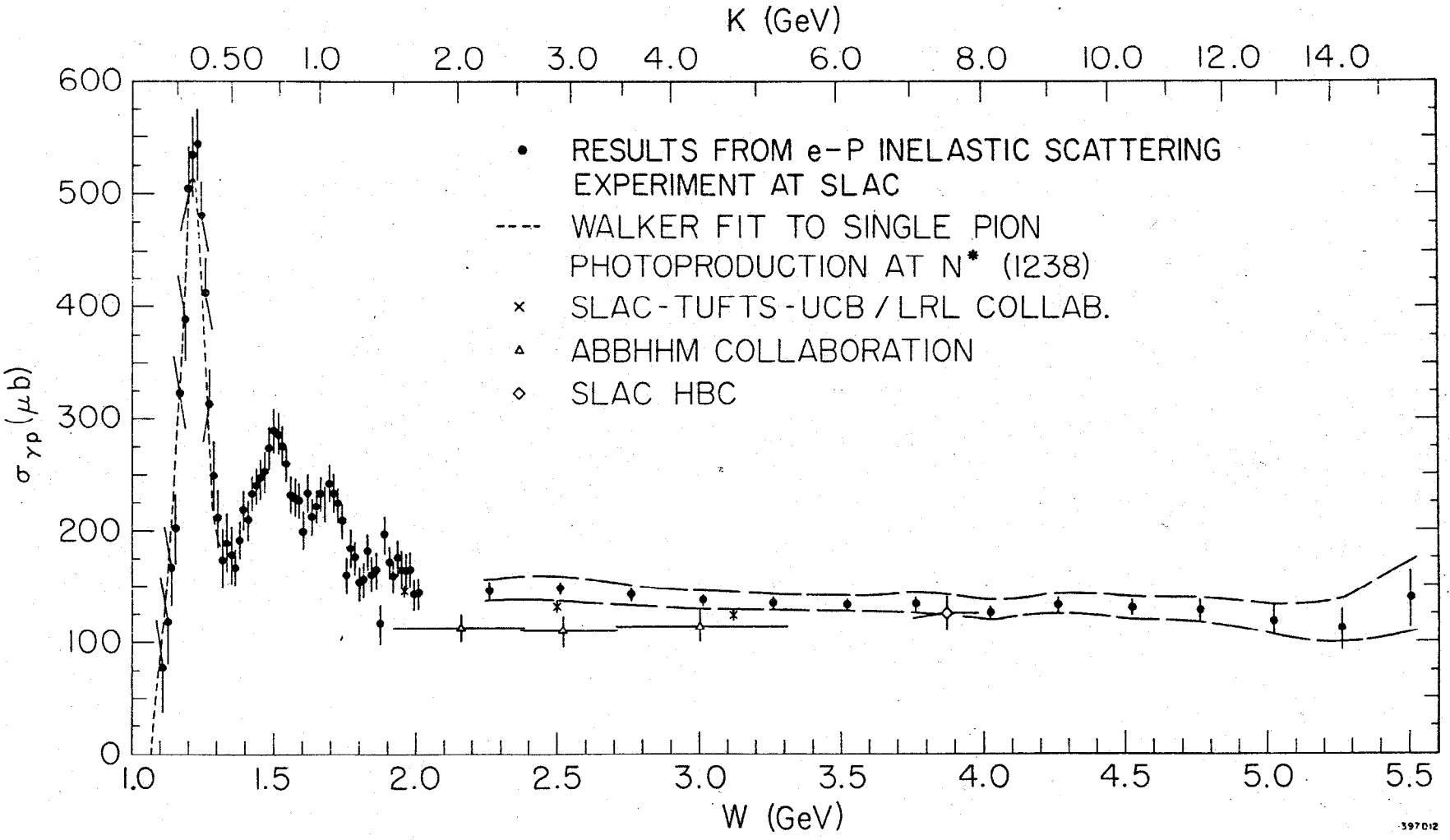
K (GeV)
0.50
1.0
2.0
3.0
4.0
6.0
8.0
10.0
12.0
14.0
600
500
400
300
200
100
0
$\sigma_{\gamma p}(\mu b)$
RESULTS FROM e-P INELASTIC SCATTERING EXPERIMENT AT SLAC
WALKER FIT TO SINGLE PION PHOTOPRODUCTION AT N* (1238)
SLAC-TUFTS-UCB / LRL COLLAB.
ABBHHM COLLABORATION
SLAC HBC
1.0
1.5
2.0
2.5
3.0
3.5
4.0
4.5
5.0
5.5
W (GeV)
397012

Fig. 18

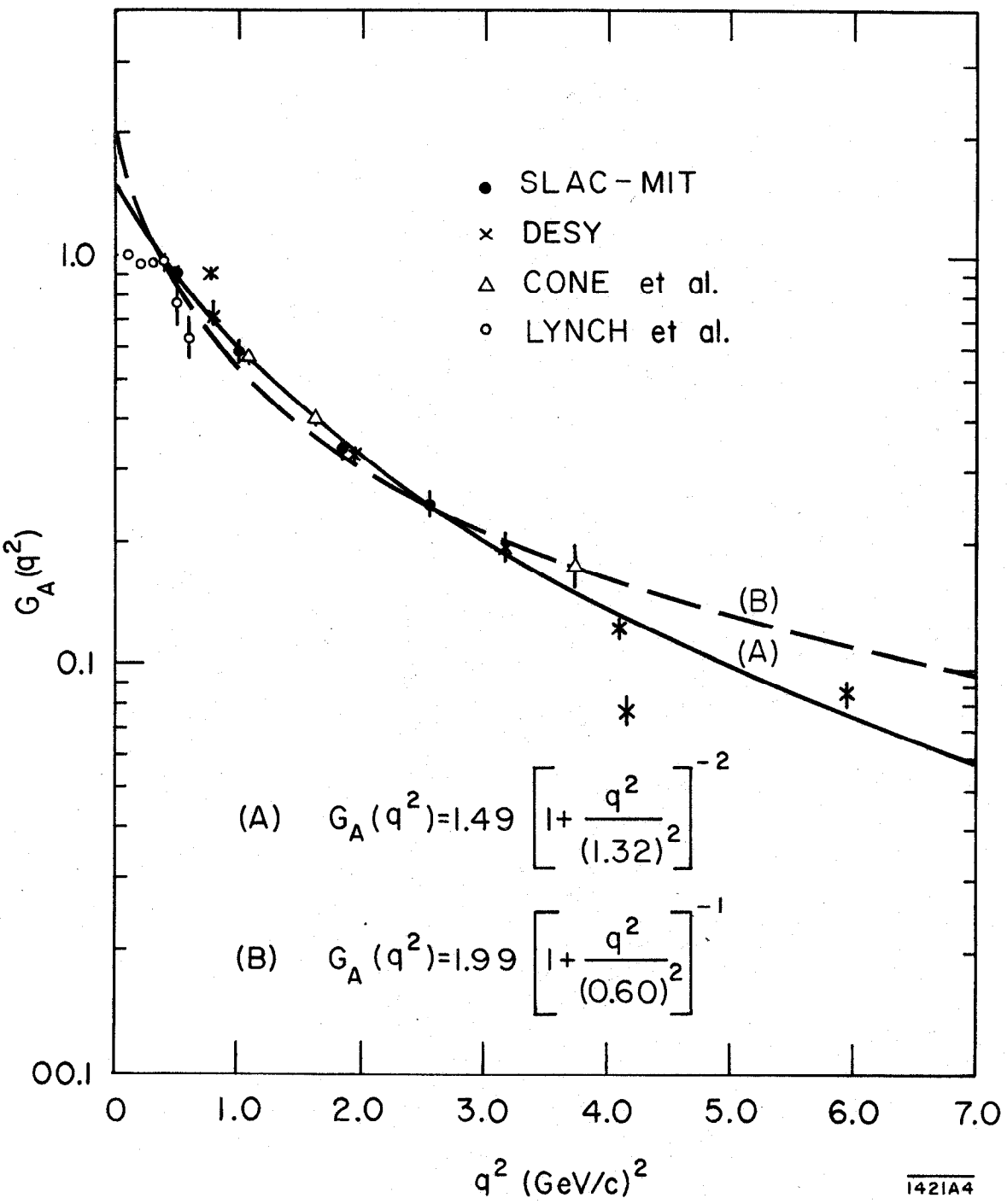
SLAC - MIT
DESY
CONE et al.
LYNCH et al.
(B)
(A)
(A) $G_A(q^2)=1.49\left[1+\frac{q^2}{(1.32)^2}\right]^{-2}$
(B) $G_A(q^2)=1.99\left[1+\frac{q^2}{(0.60)^2}\right]^{-1}$
$G_A(q^2)$
1.0
0.1
00.1
0
1.0
2.0
3.0
4.0
5.0
6.0
7.0
q^2 (GeV/c)^2
1421A4

Fig. 19